TRPV3-ANO1 interaction positively regulates wound healing in keratinocytes

山野井　遊

博士（理学）

総合研究大学院大学
生命科学研究科
生理科学専攻

平成３０（２０１８）年度

TRPV3-ANO1 interaction positively regulates wound healing in keratinocytes

Yamanoi, Yu

Doctor of Philosophy

Department of Physiological Sciences
School of Life Science
The Graduate University for Advanced Studies

2018

Index

Abstract

Transient receptor potential vanilloid 3 (TRPV3) belongs to the family of highly calcium-permeable nonselective cation channels. This channel is strongly expressed in skin keratinocytes and is involved in warmth sensation, itch, wound healing and secretion of several cytokines. Previous studies showed that anoctamin1 (ANO1), a calcium-activated chloride channel (CaCC), is activated by calcium influx through TRP vanilloid 1 (TRPV1), TRP vanilloid 4 (TRPV4) or TRP ankyrin 1 (TRPA1). These interactions between TRPs and ANO1 are important for TRP channel-mediated physiological functions. ANO1 is expressed in epithelial cells, including the choroid plexus. I found that ANO1 was expressed by normal human epidermal keratinocytes (NHEKs). Thus, I hypothesized that the physiological significance of ANO1 was linked to TRPV3 in keratinocytes. The aim of this study is to elucidate the interaction between TRPV3 and ANO1, and to investigate the physiological functions of this interaction in keratinocytes.

To clarify the functional interaction, I investigated ANO1-mediated currents upon TRPV3 activation in HEK293T cells. ANO1-mediated currents were dramatically increased through TRPV3 activation, and this event was also observed in NHEKs. Furthermore, the ANO1-mediated currents depended on extracellular calcium. These results suggested that ANO1 functionally interacted with TRPV3 in keratinocytes. In addition, direct interaction was suggested by co-immunoprecipitation. Then, I investigated the effects of an ANO1 blocker, T16Ainh-A01 (T16A), using a kind of *in vitro* wound healing assay with NHEKs. I found that T16A inhibited cell migration and proliferation. Low chloride medium (4 mM chloride) also inhibited cell migration and/or proliferation. These results indicated that chloride flux through ANO1 enhanced keratinocyte migration and/or proliferation. Furthermore, T16A or low chloride medium induced phosphorylation of p38 and c-Jun N-terminal kinase, members of the Mitogen-Activated Protein Kinase (MAPK) family. These MAPKs are cell cycle-related MAPKs. Therefore, I investigated the effect of T16A on the cell cycle using a redox dye. T16A induced cell cycle arrest. Taken together, I conclude that TRPV3-ANO1 interaction positively regulates cell migration and proliferation processes via MAPK phosphorylation and cell cycle control.

Introduction

Transient Receptor Potential (TRP) channels are comprised of six related protein families in mammals. They include TRPA (ankyrin), TRPC (canonical), TRPM (melastatin), TRPML (mucolipin), TRPP (polycystin) and TRPV (vanilloid), and many are highly calcium-permeable non-selective cation channels[1]. TRP channels are well known for their contribution to sensory transduction, such as temperature, pain, itch, touch and various other stimuli[1-9]. Consistent with the sensory function, many TRP channels (TRPA1, TRPM8, TRPM2, TRPM3, TRPV1, TRPV2 and TRPV4) are reportedly expressed in primary sensory neurons. One of the important mechanisms for TRPA1 activation is through covalent modification at cysteines at the N terminus by irritants, including allyl isothiocyanate (AITC)[10-12]. Moreover, it was recently reported that reactive oxygen species (ROS) generated from mitochondria in cold conditions sensitized TRPA1 followed by cold responses[13]. This molecular mechanism could be involved in cold hypersensitivity. TRPM8 is also involved in cool sensations because this ion channel can be activated by cool temperature and menthol analogues. The involvement of TRPM8 in cold pain sensation has been proposed[14]. TRPM2, TRPM3, TRPV1, TRPV2 and TRPV4 are known to be heat sensitive TRP channels. Although TRPM2, TRPM3 and TRPV4 can be activated by body temperature and TRPV1 and TRPV2 activities are induced by noxious heat stimulation, it is well known that TRPV1 and TRPV4 are involved in pain sensations [4,15]. Interestingly, the warm-sensitive TRP channel, TRPV4, is also expressed in the brain[16]. Depolarization through slight activation of TRPV4 enhances neuronal excitation in CA1 neurons of the hippocampus[17].

In choroid plexus epithelial cells, calcium influx activates a chloride channel, anoctamin 1 (ANO1, also called TMEM16A). Activation is followed by secretion of cerebrospinal fluid[18]. The same report showed that ANO1 was activated by calcium influx through TRPV4 and that chloride efflux through ANO1 caused the efflux of water to the apical side of choroid plexus epithelial cells. According to previous reports, other epithelial cells have both TRPV4 and ANO1. For instance, these ion channels are co-expressed in the salivary tract and salivary secretion could be accelerated by the functional interaction between TRPV4 and ANO1[19]. Recently, other interactions between TRP channels and ANO1 have been suggested. TRPC2 and ANO1 interaction could be important for iodide homeostasis in thyroid cells[20], and TRPC6 and ANO1 interaction is involved in vasoconstriction[21]. Moreover, calcium homeostasis in epithelial principal cells of the rat epididymis depends on TRPV6 and might be modulated by ANO1 activation[22]. On the other hand, the expression patterns of these ion channels are different in tracheal epithelium. There are mainly two types of cells

in the tissue, ciliary and goblet cells. Mucin secretion is enhanced by ANO1 in goblet cells[23]. TRPV4 is reportedly involved in movement of cilia[24]. Thus, TRP channel functions are modulated by ANO1 even though the function of each ion channel is physiologically significant by itself. As a result, one cannot investigate the channels' functions without their interactions when the TRP channel and ANO1 are co-expressed by the same cells.

As described above, epithelial cells are more than simple borders between the external environment and the interior of the body. Intriguingly, epithelial cells can contact primary sensory neurons by using transmitters, including ATP. ATP is released from bladder epithelial cells when TRPV4 or piezo 1 is activated by extension[23,24]. Furthermore, TRPV4 could be involved in the detection of ultraviolet B (UVB) in skin keratinocytes, and endothelin-1 release is enhanced in the skin keratinocytes exposed to UVB[25]. TRPV3 is also involved in the relationship between the skin and peripheral neurons. TRPV3 is a warm-sensitive TRP channel and calcium permeability is approximately 10 times higher than that of sodium[26]. Although TRPV3 is reportedly expressed by entire body regions, its physiological significance is not well understood except for in skin keratinocytes. Previous studies showed that TRPV3 contributed to itch, warmth sensation and wound healing in keratinocytes[27-30]. For instance, warmth-induced ATP release from keratinocytes is dependent on TRPV3 activation, but not TRPV4, and the release of ATP could activate P2X receptors in primary sensory neurons[28]. Moreover, TRPV3 activation enhanced by cell signaling downstream from the epidermal growth factor receptor accelerates warmth-dependent wound healing in oral epidermal cells[27]. In summary, these reports describe the functional expression of TRPV3 and its physiological functions. However, the molecular mechanism of wound healing in skin is still unclear because the environmental conditions between the skin and the oral cavity are different.

Body fluid homeostasis is achieved by regulating water movement across the skin. TRPV4 is involved in the skin-barrier function via formation of tight junctions and adherens junctions[31]. Furthermore, skin has an important role in protecting the body against bacterial infection following injury. Importantly, bacteria can be harmful to organisms even if they are otherwise benign on healthy skin surfaces[32]. Therefore, enhancement of wound healing is an important function. Wound healing of skin depends on cell migration and cell proliferation. Although some growth factors and interleukins are involved in wound healing[33], ion channels on plasma membranes of keratinocytes could also be important. For example, *Ano1* is reportedly a carcinoma-related gene[34,35], and a recent study revealed that ANO1 is involved in the

proliferation of prostate epithelial cells in benign prostatic hyperplasia[36]. In addition, ANO1 inhibition reduced cell migration in some cancer cells[35,37,38]. However, the physiological function of ANO1 in skin keratinocyte is not clear even though many epithelial cells express it[39]. Here, I show that ANO1 is expressed in human keratinocytes and that these channels are involved in wound healing. This study is the first report showing the significance of ANO1 in cell migration and proliferation in normal cells, but not cancer cells.

Materials and Methods

Cell Culture

HEK293T cells were maintained at 37°C in 5% CO_2 in Dulbecco's modified Eagle's medium (Wako) containing 10% fetal bovine serum (BioWest), 50 units/mL penicillin, 50 µg/mL streptomycin (Life Technologies) and 2 mM/L glutamine (GlutaMAX, Life Technologies). Normal human epidermal keratinocytes (NHEK, Adult, KURABO) were maintained at 37°C in 5% CO_2 in Humedia-KG2 (KURABO). Custom MCDB153 medium lacking NaCl (Research Institute for Functional Peptides) was used for low chloride experiments. Custom MCDB153 medium was used by adding 130 mM NaCl or 130 mM sodium aspartate and 0.1 mM O-phosphorylethanolamine (Sigma), 0.1 mM ethanolamine (Sigma), 0.5 µg/mL hydrocortisone (Sigma), 5 ng/mL epidermal growth factor (EGF, Miltenyi Biotec) and 5 µg/mL insulin (Sigma).

Chemicals

T16Ainh-A01 (T16A, Calbiochem), CaCCinh-A01 (Tocris Bioscience) and Ani9 (Sigma-Aldrich) were used as Ano1 inhibitors.

RT-PCR

Total RNA was purified from NHEKs using Sepasol-RNA I Super G (Nacalai Tesque) or RNeasy Micro (QIAGEN). Reverse transcription was performed using Super Script III reverse transcriptase (Invitrogen) for 50 min at 50°C. For investigation of mRNA expression of transient receptor potentials (TRPs), anoctamins (ANOs) and Cation-Chloride-Cotransporters (CCCs) in NHEKs, DNA fragments were amplified using EmeraldAmp PCR Master Mix (TAKARA) with PCR primers shown in Table 1. The PCR products were confirmed by electrophoresis on 2% agarose gel containing ethidium bromide.

Western blotting

Proteins were extracted from NHEKs treated with 10 µM T16A or low chloride medium or control medium for 13 h. The cells were washed with cold PBS and lysed by treatment with lysis buffer (1% Triton X-100 contained 150 mM NaCl, 10 mM Tris-HCl, 1 mM EDTA, 1 mM Na_3VO_4 and protease inhibitor cocktail, cOmplete (Roche), pH 7.5). Following centrifugation at 10,000 g for 30 sec, the supernatants were denatured by treatment with SDS buffer containing 0.5 M Tris-HCl, 10% sodium dodecyl sulfate, 6% ß-mercaptoethanol, 10% glycerol, 0.01% bromophenol blue, 100 mM dithiothreitol, at

90°C for 5 min. The protein samples were used in SDS-PAGE. Blotting was done with rabbit anti-ANO1 antibody (Abcam, ab53213, 1:5), rabbit anti-phospho-ERK (extracellular signal-related kinase) antibody (Cell Signaling Technology, #4370, 1:1000), rabbit anti-phospho-p38 antibody (Cell Signaling Technology, #4511, 1:1000), rabbit anti-phospho-JNK (c-Jun N-terminal Kinase) antibody (Cell Signaling Technology, #4668, 1:1000), rabbit anti-ERK antibody (Cell Signaling Technology, #4695, 1:1000), rabbit anti-p38 antibody (Cell Signaling Technology, #8690, 1:1000), rabbit anti-JNK antibody (Cell Signaling Technology, #9252, 1:1000), mouse anti-β-actin antibody (Abcam, ab6276, 1:2500), anti-rabbit-HRP antibody (Cell Signaling Technology, #7074, 1:2000) and anti-mouse-HRP antibody (Cell Signaling Technology, #7076, 1:2000).

Transfection

Transient transfection of HEK293 cells was achieved with Lipofectamine Transfection Reagent (Life Technologies), PLUS Reagent (Life Technologies) and Opti-MEM I Reduced Serum Medium (Life Technologies). Plasmid DNAs (hTRPV6/pcDNA3.1, hTRPV3/pcDNA3, hANO1/pcDNA3.1 or pcDNA3.1) were transfected with pGreen Lantern 1 into HEK293T cells, and the transfected cells were used for patch-clamp recording and immunoprecipitation 16–30 h after transfection.

Calcium imaging

NHEKs on coverslips were incubated at 37°C for 30 min in Humedia-KG2 containing 5 μM Fura-2-acetoxymethyl ester (Molecular Probes). The cover slips were washed with a standard bath solution containing 140 mM NaCl, 5 mM KCl, 2 mM $CaCl_2$, 2 mM $MgCl_2$, 10 mM HEPES and 10 mM D-glucose at pH 7.4, adjusted with NaOH. A calcium-free bath solution was prepared by omitting 2 mM $CaCl_2$ from the standard bath solution and adding 5 mM EGTA. Fura-2 was excited with 340- and 380-nm wavelength lights and the emission was monitored at 510 nm with a CCD camera, Cool Snap ES (Roper Scientific/Photometrics) at room temperature. Data were acquired using IP lab software (Scanalytics) and analyzed with ImageJ software (National Institutes of Health). Ionomycin (5 μM, Sigma-Aldrich) was applied to confirm the maximal response of each cell. High K^+ bath solution contained 65 mM NaCl, 80 mM KCl, 2 mM $CaCl_2$, 2 mM $MgCl_2$, 10 mM HEPES and 10 mM D-glucose at pH 7.4, adjusted with NaOH.

Whole cell patch-clump

Transfected HEK293T cells or NHEKs were used for whole-cell recordings. Patch

pipettes were made from borosilicate glass (type 8250, King Precision Glass) with a five-step protocol using a P-2000 (Sutter Instrument). The pipette resistance was 3-8 MΩ. Currents were recorded at 10 kHz using an Axopatch 200B amplifier (Molecular Devices) and filtered at 5 kHz with a low-pass filter. Currents were digitized with a Digidata 1440A or 1550 (Axon Instruments). Data acquisition was achieved with pCLAMP 10 software (Axon Instruments). Four extracellular solutions for whole-cell recording were as follows: (1) a standard bath solution (140 mM NaCl, 5 mM KCl, 2 mM $CaCl_2$, 2 mM $MgCl_2$, 10 mM HEPES and 10 mM D-glucose at pH 7.4, adjusted with NaOH); (2) an NMDG-Cl bath solution (140 mM NMDG, 140 mM HCl, 2 mM $CaCl_2$, 2 mM $MgCl_2$, 10 mM HEPES and 10 mM D-glucose at pH 7.4, adjusted with HCl); (3) a calcium-free NMDG-Cl bath solution that was prepared by omitting 2 mM $CaCl_2$ from the NMDG-Cl bath solution and adding 5 mM EGTA and (4) an NMDG-aspartate bath solution that was prepared by using L-aspartic acid instead of HCl. The pipette solutions were as follows: (1) a standard pipette solution (140 mM KCl, 5 mM EGTA, 2 mM $MgCl_2$ and 10 mM HEPES at pH 7.3, adjusted with KOH) or (2) an NMDG-Cl pipette solution (140 mM NMDG, 140 mM HCl, 5 mM BAPTA, 2 mM $MgCl_2$ and 10 mM HEPES at pH 7.3, adjusted with HCl). $CaCl_2$ was added to the pipette solution so that the free calcium concentration was 100 nM. Free calcium concentrations were calculated with the MAXC program of Stanford University.

I used the following solutions for voltage-gated calcium channel experiments. Voltage-gated calcium channel: bath solution contained 145 mM NMDG, 145 mM HCl, 5 mM EGTA, 2 mM $MgCl_2$, 10 mM HEPES and 10 mM D-glucose at pH 7.4, adjusted with HCl. $BaCl_2$ was added to bath solution so that the free barium concentration was 2 mM. NMDG-Cl pipette solution was used without $CaCl_2$.

Immunoprecipitation

Proteins were extracted from HEK293T cells after transfection. The cells were lysed as described above. Following centrifugation at 16,100 g for 30 min, the supernatants were incubated in a rotator for 2 h with protein G Mag Sepharose (GE Healthcare). After removal of magnetic beads, the supernatants were incubated in a rotator overnight with rabbit anti-TRPV3 antibody (Cell Signaling Technology, #3484, 1:50) or rabbit anti-ANO1 antibody (Abcam, ab53212, 1:00). After incubation, protein G Mag Sepharose was added, and the solutions were incubated in a rotator for 2 h. After incubation, the magnetic beads were rinsed with washing buffer (50 mM Tris-HCl, 150 mM NaCl, pH7.5). The proteins were denatured by SDS buffer at 95°C for 5 min. The protein samples were assessed by SDS-PAGE. Blotting was done by rabbit

anti-TRPV3 antibody (Cell Signaling Technology, #3484, 1:1000) and anti-rabbit-HRP antibody (Cell Signaling Technology, #7074, 1:2000).

DNA microarray

NHEKs were cultured in low chloride medium, 10 μM T16A-containing medium or MCDB153 medium (control) for 13 h. Total RNA was purified from the NHEKs using FastGene RNA Premium Kit (NIPPON Genetics) and analysed by SurePrint G3 Human Gene Expression 8x60K v3 (Takara Bio).

Culture insert assay

NHEKs were seeded confluently in 2-well culture inserts (ibidi) on glass-bottom dishes (Matsunami). Culture-inserts were removed after overnight incubation, followed by washing with PBS. Cells were then cultured in Humedia-KG2, MCDB153 medium or low chloride MCDB153 medium. After 12 or 24 h of cultivation, calcein-AM (Dojindo) was added to the culture medium to visualize the cells. ImageJ software was used for data analysis. For time-lapse analysis, cells were cultured in a Stage Top Incubator (TOKAI HIT) on a confocal laser scanning microscope (IX83 Olympus) and images were captured every 10 min.

MTT assay

NHEKs were seeded on 96-well plates (Falcon). Cells were cultured in control medium, 10 μM, 5 μM or 2.5 μM T16A-containing medium for 24 h or 48 h. After culture, MTT assays were done using an MTT Cell Proliferation Assay Kit (Cayman). Absorbance of the formazan was measured with a microplate reader (Multiskan Spectrum, Thermo Fisher) at 570 nm.

Chloride imaging

NHEKs were seeded on glass bottom dishes (Matsunami). Cells were incubated with 10 mM MQAE (chloride ion-quenched fluorescent indicator, Dojindo) for 60 min at 37°C in a Stage Top Incubator (TOKAI HIT) on a confocal laser scanning microscope (LSM 510META, Carl Zeiss). MQAE was excited at 780 nm using a two-photon excitation laser system (Mai Tai, Spectra-Physics), and emission was at 458-479 nm.

The 0 mM chloride calibration solution contained 10 mM $NaNO_3$, 140 mM KNO_3, 0.5 mM $Ca(NO_3)_2$, 0.5 mM $Mg(NO_3)_2$, 10 mM HEPES, 5 mM D-glucose at pH 7.4, adjusted with CsOH. The 100 mM chloride calibration solution contained 10 mM $NaNO_3$, 100 mM KCl, 40 mM KNO_3, 0.5 mM $Ca(NO_3)_2$, 0.5 mM $Mg(NO_3)_2$, 10 mM HEPES, 5 mM

D-glucose at pH 7.4, adjusted with CsOH. The 50 mM chloride calibration solution was made by mixing 0 mM and 100 mM chloride calibration solution 1:1. Each calibration solution was used by adding nigericin (monovalent cation ionophore), valinomycin (potassium ionophore) and tributyltin (chloride ionophore) so that final concentrations were 5 μM, 10 μM and 10 μM, respectively. All experiments were done at 37°C.

Cell cycle assay

NHEKs were seeded in the same way as the wound-healing assay. After removing the culture insert at 12 h, cells were stained with a Cell-Clock Cell Cycle Assay Kit (Biocolor). ImageJ software was used for data analysis. The distribution of cell cycle phases were defined as the threshold color. G2/M phase (dark blue) cells were defined as Hlu 0-255, Saturation 40-255, Brightness 0-90. S phase (green) cells were defined as Hlu 70-255, Saturation 40-255, Brightness 90-255. G0/G1 phase (yellow green) cells were defined as Hlu 0-70, Saturation 40-255, Brightness 90-255.

Results

4-1. Expression of TRPs and ANOs in normal human epidermal keratinocytes

The status of endogenous gene expression of TRP channels and ANOs was unclear in NHEKs. To clarify the expression patterns, I performed RT-PCR analysis of cultured NHEKs (Fig. 1A). While previous reports suggested that TRPV1, TRPV3, TRPV4, TRPV6 proteins were expressed in keratinocytes[40], mRNAs of *TRPV1*, *TRPV2*, *TRPV3*, *TRPV4*, *TRPV6, ANO1, ANO4, ANO9* and *ANO10* were detected in my hand (Fig. 1A). Although ANO2 is also a calcium-activated chloride channel (CaCC), a clear band with the predicted molecular weight was not detected in NHEKs. In contrast, ANO1 protein expression was observed by Western blotting (Fig. 1B). These results suggested significant expression of ANO1 in NHKEs. Additionally, I performed calcium-imaging experiments using Fura-2 to investigate functional expression of TRP channels. Whereas camphor (10 mM, a TRPV3 agonist) and GSK1016790A (300 nM, a TRPV4 agonist) obviously induced intracellular calcium increases in all cells, capsaicin (300 nM to 3 μM, a TRPV1 agonist), probenecid (100 μM, a TRPV2 agonist), allyl isothiocyanate (AITC, 100 μM or 1 mM, a TRPA1 agonist), menthol (100 μM, a TRPM8 agonist) and 1-oleoyl-acetyl-sn-glycerol (OAG, 90 μM, a TRPC6 agonist) did not produce clear responses (Fig. 1C). I also performed calcium-imaging experiments using calcium-free extracellular medium because intracellular calcium concentrations are supposed to be reduced upon removal of extracellular calcium in cells expressing TRPV6, which can be constitutively active. However, the intracellular calcium concentrations were not different in the presence or absence of extracellular calcium (Fig. 1D). Additionally, a typical current with inward rectification by TRPV6 activation was not observed in NHEKs (Fig.1E). These results indicated that the most functional TRP channels were TRPV3 and TRPV4, although expression of other TRP channel was suggested in RT-PCR experiments. Thus, ANO1 could be activated by calcium influx through TRPV3 and TRPV4 in cells that co-expressed these ion channels. Therefore, I decided to focus on the interaction between TRPV3 and ANO1 in this study because their interaction had not received attention in the literature.

4-2. TRPV3-ANO1 interaction in HEK293T cells

I performed whole cell patch-clamp experiments using HEK293T cells heterologously expressing TRPV3 and ANO1 to investigate their functional interaction. NMDG-Cl bath and pipette solutions were used to identify chloride currents through ANO1 because NMDG is known not to permeate pores of cation channels. I used camphor as a TRPV3 agonist since a previous report showed other TRPV3 agonists, 2-APB and

carvacrol, inhibited ANO1 currents[41]. Under these conditions, chloride currents were clearly observed in cells expressing human TRPV3 (hTRPV3) and human ANO1 (hANO1), but not in cells expressing hTRPV3 or hANO1 alone (Fig. 2A, B). The currents were interpreted to be chloride currents passing through hANO1 that had been activated by calcium entering cells through hTRPV3. The currents were observed with intracellular 1, 2-bis (o-aminophenoxy) ethane-N,N,N',N'-tetraacetic acid (BAPTA) (5 mM), which is a relatively strong calcium chelator. Thus, this result suggested that TRPV3-ANO1 interaction could occur in a local calcium nanodomain in which BAPTA-mediated calcium chelation did not function. Previous studies suggested that both TRPV1 and TRPV4 physically interacted with ANO1[18,19,42]. Therefore, I performed immunoprecipitation and Western blotting experiments using anti-ANO1 and anti-TRPV3 antibodies, respectively, with extracts from HEK293T cells (Fig.2C). There were no TRPV3 bands in negative control extracts from cells transfected with *hANO1* cDNA, *hTRPV3* cDNA or pcDNA3.1 plasmid alone. The results indicated that hTRPV3 physically interacts with ANO1. These results suggested that the functional interaction between hTRPV3 and hANO1 in the heterologous expression system occurs in calcium nano-domain just under a plasma membrane expressing hTRPV3 and hANO1.

4-3. TRPV3-ANO1 interaction in NHEKs

Intracellular calcium increases were observed in all NHEKs upon camphor application (Fig. 1C). Therefore, I performed whole-cell patch-clamp experiments in NHEKs. Camphor-induced chloride currents were observed in 148 mM chloride-containing bath solution (Fig. 3A). In this experiment, the BAPTA concentration in the pipette solution was 5 mM. The reversed potential of the chloride currents was shifted to a positive direction when the extracellular chloride concentration was changed to 4 mM (Fig.3B, C). That result indicated that chloride was a major ion carrier of the camphor-induced currents. Calcium releases from the endoplasmic reticulum might not be a major contributor to increases in intracellular calcium concentrations in NHEKs because the increase in intracellular calcium concentrations was small in the calcium-free bath solution (Fig.3D). This interpretation was confirmed in patch-clamp experiments in which the camphor-induced currents were very small in the extracellular calcium-free solution (Fig. 3E). Therefore, TRPV3 agonist-induced chloride currents through ANO1 in NHEKs mainly depend on the calcium influx through TRPV3 from extracellular regions.

There was no inhibition of TRPV3 or TRPV4 activities following application of

T16Ainh-A01 (T16A), an ANO1 inhibitor, in the calcium-imaging experiments. In contrast, another ANO1 inhibitor, CaCCinh-A01 reduced the activities of both TRPV3 and TRPV4 (Fig. 4). In the calcium imaging experiments, the activity of TRPV3 was not inhibited by addition of Ani9, another strong ANO1 inhibitor (Fig. 4). Therefore, I used T16A or Ani9 as ANO1 inhibitors in the following experiments. The camphor-induced chloride currents were inhibited by Ani9 (Fig. 3F). This result suggested TRPV3-ANO1 interaction in NHEKs.

ANO1 is reportedly activated by activation of voltage-gated calcium channels[43], and previous studies showed the expression of some voltage-gated ion channels in keratinocytes[44-46]. Therefore, activation of ANO1 could possibly be caused, in part, by intracellular calcium increases downstream of the activation of voltage-gated calcium channels. To investigate this possibility, I executed whole-cell patch-clamp recordings of voltage-gated calcium channels (Fig. 5). However, no barium currents were observed upon the membrane potential changes. Furthermore, no intracellular calcium increases were induced by application of a high potassium solution in the calcium-imaging experiments (Fig. 5B). These results suggested there was no functional expression of voltage-gated calcium channels.

4-4. Effects of an ANO1 inhibitor or low chloride medium in a kind of wound-healing assays of NHEKs

Previous studies showed that TRPV3 contributes to itch and warmth sensations and wound healing by keratinocytes[27-30]. It has been strongly suggested that TRPV3 activation accelerates wound healing in the oral cavity[27]. Moreover, the basic histological properties of the oral cavity are similar to those of skin compared to other mucosa in the body[47]. Furthermore, ANO1 could be involved in tissue development after birth[48], and it is well-known to be a positive regulator of migration and proliferation in cancer cells[34,35,37,38]. Therefore, I hypothesized that TRPV3-ANO1 interaction might affect the migration and/or proliferation of NHEKs and the process of wound healing. Indeed, DNA microarray analyses showed that T16A or low chloride conditions decreased positive regulators of wound healing such as *MMP7* (matrix metalloproteinase 7), *CXCL10* (C-X-C motif chemokine ligand 10), *IGF2* (insulin like growth factor 2) and *NOS2* (nitric oxide synthase 2) in NHEKs (Fig. 6 and Table 2). To investigate the involvement of ANO1 in wound healing, I analyzed the effects of an ANO1 blocker, T16A, in a kind of *in vitro* wound healing assay through the use of a culture insert (Fig.7). In this experiment, NHEKs were cultivated within a culture insert at almost 100 % confluency in which cells migrated to spaces between cell

clusters[49] (Fig. 7A). NHEKs usually migrated to the open spaces, an area separated by the insert, for approximately 12 h after the insert was removed. In this way, migration and proliferation filled the area by about 80% within 24 h. However, cell migration and/or proliferation in 5 μM T16A-containing medium was obviously inhibited although the inhibition was gone after washout of T16A (Fig. 7B, C), suggesting that the T16A effect was not due to cell-death or irreversible cell damage. In addition, I analyzed cell migration velocity using time-lapse imaging with a confocal microscope and cell proliferation using an MTT assay (Fig. 7D-F). Migration velocity was reduced after T16A application, and the reduction lasted throughout the continued presence of ANO1 inhibition (Fig. 7D). Moreover, the migration velocity recovered to the initial level after washout of T16A (Fig. 7D and E). Cell proliferation was also reduced by T16A application (Fig. 7F).

The above experiments were performed at 37°C, and TRPV3 is thought to be activated in this condition. According to a previous report, ANO1 is also activated by rapid noxious heat stimulation[50]. However, another group reported that ANO1 was activated by the temperature increase without a clear threshold for temperature-evoked activation in a physiological intracellular free-calcium concentration (100 nM)[18]. Thus, ANO1 is also thought to be activated in this condition. Therefore, I investigated temperature-dependency in the assay with a culture insert as described above (Fig. 8). The filled areas after the removal of the culture insert were significantly smaller with a reduction of temperature from 37 to 30˚C within which TRPV3 and TRPV4 are reportedly activated[51-54] regardless of the presence of T16A (Fig. 8). These data suggested that changes in the filled areas involve temperature-dependent mechanisms that could be due to activation of temperature-dependent molecules such as TRPV3, TRPV4 or ANO1.

The results shown in Figure 7 suggested the importance of chloride ions for cell migration and proliferation. Therefore, I performed an assay with a culture insert in low chloride medium at 37˚C (Fig. 9). Intracellular chloride concentrations should be reduced upon depletion of extracellular chlorides[55]. After removal of the culture insert, the filled areas were drastically reduced in the low chloride-containing medium, an effect that was lost after the change to the control medium (Fig. 9). These results indicated that chloride flux through ANO1, possibly influx, plays critical roles in cell migration and/or proliferation.

4-5. Direction of chloride movement through chloride channels in NHEKs

Although the previous results suggested the importance of chloride ions for cell

migration and/or proliferation, the actual roles of chloride ions in keratinocytes are largely unknown. To address this question, I attempted to determine the direction of chloride movement. Chloride permeation through chloride channels depends on intracellular chloride concentrations and membrane potentials. Although chloride channel function could affect intracellular chloride concentrations, they should be maintained by the function of several chloride transporters[56]. Therefore, I examined the expression patterns of chloride transporters, including Na-K-Cl cotransporters (NKCCs) and K-Cl cotransporters (KCCs) using RT-PCR. In this experiment, the expression of *NKCC1*, *KCC1*, *KCC2*, *KCC3* and *KCC4* mRNAs was suggested (Fig. 10A). KCC2 is a neuron-specific KCC, and intracellular chloride concentrations are kept at a low level through chloride efflux by KCC2 in cells in the central nervous system. It is believed that opening of the chloride-permeable channels causes chloride influx. Therefore, I performed a chloride-imaging experiment using a chloride indicator, MQAE[57-59]. The calculated intracellular chloride concentrations of NHEKs (6.8 ± 1.3 mM) were relatively low, which is consistent with the relatively high *KCC2* expression at least at the mRNA level in NHEKs. The equilibrium potential for chloride ions was -75.7 mV (Fig. 10B,C). The fact that the reported resting membrane potentials of skin keratinocytes are -24 to -40 mV[60-62] suggested that chloride influx occurs through ANO1 in NHEKs.

4-6. An ANO1 inhibitor or a low chloride condition induces MAP kinase phosphorylation

Previous studies suggested that low intracellular chloride concentrations induce the phosphorylation of mitogen-activated protein kinase (MAPK), although its precise mechanisms are not well known. MAPK cascades are involved in the life and death of many cells[63,64] (Fig. 11A). For instance, extracellular signal-related kinase (ERK), which is phosphorylated by MAPK kinase (MKK)1/2, is involved in cell proliferation and differentiation. On the other hand, p38 and c-Jun N-terminal kinase (JNK), which are phosphorylated by MKK3/4/6 and MKK4/7, respectively, induce cell cycle arrest and apoptosis. Hence, I investigated MAPK phosphorylation using a Western blot method (Fig. 11B). An ANO1 inhibitor, T16A or a low chloride condition increased phosphorylation of p38 and JNK, but not that of ERK. These results suggested that ANO1 is involved in cell cycle arrest and/or apoptosis. However, neither ANO1 inhibition nor a low chloride condition induced cell death in the culture insert assay based upon the fact that cell appearance visualized with a calcein-AM staining was not affected by ANO1 inhibition or a low chloride condition (Figs. 7-9). In addition, there were no effects of T16A treatment on the expression of differentiation-related genes,

including *K1*, *IVL* and *TGM1*, in both differentiated and undifferentiated conditions (Fig. 12). This result is consistent with the lack of effects of the T16A treatment on ERK phosphorylation (Fig. 11B), which is known to be related to differentiation (Fig. 11A). Therefore, I decided to focus on cell cycle arrest.

4-7. An ANO1 inhibitor induced cell cycle arrest during the culture insert assay

Because the MAPK analyses suggested cell cycle arrest by ANO1 inhibition, I performed a cell cycle assay by using a redox dye (Fig. 13). Redox conditions are closely related to the cell cycle[65]. For instance, intracellular redox conditions in cells in the G0/G1 phases are relatively reductive, whereas redox conditions are gradually shifted to more oxidative ones upon progression to G2/M phases. In this assay system, cells at G0/G1 phases, S phase, and G2/M phases can be visualized as yellow green, green and dark blue, respectively (Fig. 13A). To clarify the color variation, each cell was visualized as a red color depending on signal levels (Fig. 13B). T16A treatment increased cell populations in G0/G1 phases and reduced cell populations in the S phase during the culture insert assay (Fig. 13B, C). This result indicated that cell cycle progression from G0/G1 phases to S phase was suppressed by ANO1 inhibition.

Discussion

In contrast to previous studies, my results showed that functional expression of TRPs was limited, although mRNA expression for a number of TRPs was observed in NHEKs. Functional expression was limited to TRPV3 and TRPV4 (Fig. 1). Protein expression is reported to change depending on differentiation conditions in keratinocytes[66]. Thus, TRPs whose functional expression was not confirmed in our experiments could be functional in other specific differentiation conditions. In particular, TRPV6 and TRPC6 were reported to be involved in keratinocyte differentiation, and TRPC6 expression was increased by stimulation of differentiation[67,68]. ANO1 mRNA expression was observed under both differentiated and undifferentiated conditions (Fig. 12). While I observed TRPV3-ANO1 interaction in this study and my laboratory reported similar results for TRPV4-ANO1 in epithelial cells[18, 19], interaction between ANO1 and other TRPs whose functional expression was not confirmed in this study might be present under differentiated conditions.

Several studies, including ones in my laboratory, showed that TRPV1, TRPV4, TRPV6, TRPA1, TRPC2 and TRPC6 interact with ANO1. The fact that TRPV6 and TRPC6 were reported to be involved in keratinocyte differentiation raises the possibility that ANO1 could play a role in the differentiation process. However, it seems unlikely based on my experiments since functional expression of TRPV6 and TRPC6 was not observed (Fig. 1), and the expression patterns of differentiation-related genes were not different between control and ANO1 inhibitory conditions (Fig. 12).

TRPV4 was the TRP channel that was known to interact with ANO1 in NHEKs, and TRPV3 was found to be a new candidate partner of ANO1. Therefore, I focused on clarification of the novel TRPV3-ANO1 interaction in keratinocytes. Patch-clamp experiments showed TRPV3-ANO1 interaction in HEK293T cells and NHEKs (Figs 2, 3). In addition, TRPV3 was co-immunoprecipitated using an anti-ANO1 antibody in HEK293T cells expressing both TRPV3 and ANO1. These results suggest that TRPV3 and ANO1 form a complex with a calcium nano-domain and that ANO1 is effectively activated by calcium entering cells through TRPV3 as is the case with TRPV4. It is known that increases in intracellular calcium concentrations downstream of activation of calcium-sensing receptor (CaSR) induce differentiation in keratinocytes[69]. Thus, there could be two different types of increases in intracellular calcium concentrations: a local one through TRPV3 activation that activates ANO1 and a global one that can be caused by several mechanisms such as CaSR signaling.

Next, I assessed the physiological function of TRPV3-ANO1 interaction. A previous study showed that TRPV3 was involved in wound healing in keratinocytes[27]. In fact,

TRPV3 is sensitized by epidermal growth factor receptor (EGFR) following stimulation by EGF released during wound healing. In addition, transforming growth factor alpha (TGFα), an EGFR ligand, is released from keratinocytes by TRPV3 activation. This autocrine system is thought to represent one of the molecular mechanisms for wound healing via TRPV3 activity. My assays with culture inserts suggest that ANO1 inhibition reduces cell migration and proliferation (Fig. 7). Thus, TRPV3-ANO1 interaction could be an important molecular mechanism for wound healing in skin, suggesting that there are two mechanisms for wound healing that involve TRPV3 activity. Furthermore, a previous report suggested that membrane localization of ANO1 is important for cancer cell migration, independent of the activity of chloride channel activity[70]. However, my results showed that low chloride conditions inhibited cell migration and/or proliferation in culture insert assays (Fig. 9). This result suggests that chloride movement through ANO1 is important for wound healing.

The direction of chloride movement is strictly regulated by the balance of intracellular chloride concentration and membrane potential. In mature neurons of the central nervous system, low intracellular chloride concentrations are maintained by KCC2[56]. Thus, the activation of chloride channels induces chloride influx followed by hyperpolarization. On the other hand, primary sensory neurons and immature neurons in the brain have high intracellular chloride concentrations[56,71]. Therefore, chloride channel opening induces chloride efflux at resting potentials, causing membrane depolarization. Basal intracellular chloride concentrations are controlled by chloride transporters[56]. Expressions of *NKCC1*, *KCC1, KCC2, KCC3* and *KCC4* were observed in the RT-PCR analyses of NHEKs (Fig. 10A). Furthermore, for the first time, basal intracellular chloride concentrations in keratinocytes were found to be low in my study (Fig. 10B). Because the resting membrane potentials of skin keratinocytes are reported to range from -24 to -40 mV[60-62], ANO1 opening should induce chloride influx in NHEKs. Therefore, ANO1 inhibition likely decreases intracellular chloride ions within keratinocytes. Although KCC2 is thought to be neuron-specific[72], a recent report showed that pancreatic β cells also have KCC2[73], suggesting that KCC2 might be expressed more widely than expected. Since both keratinocytes and neurons are ectodermal cells in origin[74,75], there is a possibility that neuron-specific KCC2 could control intracellular chloride concentrations in keratinocytes.

In cancer cells, decreases in intracellular chloride concentrations induce phosphorylation of p38 and JNK. That change in turn increases p21 expression, leading to the inhibition of CDK2/Cyclin E complex function, followed by arrest of the cell cycle

in the G1 phase[76,77]. Consistent with the previous reports in cancer cells, p38 and JNK phosphorylation was induced by ANO1 inhibition or low chloride conditions in NHEKs (Fig. 11). p38 and JNK are generally known to negatively regulate the cell cycle[63]. Therefore, this result together with the reduction in cell proliferation by ANO1 inhibition shown in the MTT assay (Fig. 7F) suggest that ANO1 inhibition causes cell cycle arrest. As expected, T16A treatment increased cells at the G0/G1 phases and reduced cells in the S phase as determined in the culture insert assay condition (Fig. 13B, C). That outcome indicated cell cycle arrest between the G0/G1 phases and the S phase, which is consistent with the data in previous studies that showed cell cycle arrest at the G1/S checkpoint by intracellular low chloride concentrations in cancer cells[76,77]. Thus, these results suggest that the cell cycle of keratinocytes also could be controlled by changes in intracellular chloride concentrations downstream of TRPV3-ANO1 signaling.

A previous study showed that TRPV3 in keratinocytes participates in wound healing. My study suggests that TRPV3 induces chloride influx through ANO1. This chloride influx could maintain the cell cycle properly through its inhibition of p38 and JNK phosphorylation. Thus, the decreases in cell proliferation caused by T16A (Fig. 7F) could be partly explained by the cell cycle arrest through ANO1 inhibition. My data also showed that ANO1 inhibition slowed cell migration (Fig. 7D, E). The mechanisms for controlling migration velocity by ANO1 are unknown. However, previous reports showed that molecules inhibiting the cell cycle such as p21 rearrange the cytoskeleton through an ROS-mediated pathway, resulting in the regulation of cell migration[78]. Thus, chloride could also control cell migration through the same molecules that inhibit the cell cycle. Indeed, DNA microarray analyses showed that T16A or low chloride conditions decreased positive regulators of wound healing such as *MMP7*, *CXCL10, IGF2* and *NOS2* (Fig. 6, Table 2)[79-82]. These wound healing-related genes could also be candidate regulators for cell migration.

The exact mechanism by which chloride regulates MAPK phosphorylation is unknown. A previous study showed that intracellular chloride concentrations directly affected phosphatase activity[83]. This mechanism could explain MAPK phosphorylation. DNA microarray analyses showed a decrease of WNK (lysine deficient protein kinase) 2 during T16A treatment or low chloride conditions in NHEKs (Table 2). WNK1 is also expressed in keratinocytes in my study and in a previous report,[84] although its expression level was not significantly affected by T16A treatment or low chloride conditions in NHEKs (Table 2). The activities of the WNK family of proteins, which are reportedly involved in MAP kinase phosphorylation, are regulated by intracellular

chloride[85,86]. These chloride-sensitive molecules are also candidates for proteins upstream of MAPK. Further studies are necessary to clarify the roles of chloride in cell signaling pathways of keratinocytes. Nonetheless, the interaction of TRPV3 and ANO1 found in my study suggests that together they could positively regulate keratinocyte proliferation and migration during wound healing. That interaction would be a promising starting point to investigate the detailed mechanisms through regulation of intracellular chloride concentrations.

Acknowledgements

I would like to thank Dr. Shigekuni Hosogi (Kyoto Prefectural Univ.) for support of chloride imaging. I am grateful to Prof. Makoto Tominaga for encouragement and supervision throughout the course of my doctoral thesis. I also thank Dr. Yasunori Takayama for kind advice and guidance of my study. I would like to thank all laboratory members as well.

References

1 Venkatachalam, K. & Montell, C. TRP channels. *Annu Rev Biochem* **76**, 387-417, doi:10.1146/annurev.biochem.75.103004.142819 (2007).

2 Caterina, M. J., Rosen, T. A., Tominaga, M., Brake, A. J. & Julius, D. A capsaicin-receptor homologue with a high threshold for noxious heat. *Nature* **398**, 436-441, doi:10.1038/18906 (1999).

3 Caterina, M. J. *et al.* The capsaicin receptor: a heat-activated ion channel in the pain pathway. *Nature* **389**, 816-824, doi:10.1038/39807 (1997).

4 Grant, A. D. *et al.* Protease-activated receptor 2 sensitizes the transient receptor potential vanilloid 4 ion channel to cause mechanical hyperalgesia in mice. *J Physiol* **578**, 715-733, doi:10.1113/jphysiol.2006.121111 (2007).

5 McKemy, D. D., Neuhausser, W. M. & Julius, D. Identification of a cold receptor reveals a general role for TRP channels in thermosensation. *Nature* **416**, 52-58, doi:10.1038/nature719 (2002).

6 Naziroglu, M., Ozgul, C., Celik, O., Cig, B. & Sozbir, E. Aminoethoxydiphenyl borate and flufenamic acid inhibit Ca2+ influx through TRPM2 channels in rat dorsal root ganglion neurons activated by ADP-ribose and rotenone. *J Membr Biol* **241**, 69-75, doi:10.1007/s00232-011-9363-9 (2011).

7 Peier, A. M. *et al.* A TRP channel that senses cold stimuli and menthol. *Cell* **108**, 705-715 (2002).

8 Story, G. M. *et al.* ANKTM1, a TRP-like channel expressed in nociceptive neurons, is activated by cold temperatures. *Cell* **112**, 819-829 (2003).

9 Vriens, J. *et al.* TRPM3 is a nociceptor channel involved in the detection of noxious heat. *Neuron* **70**, 482-494, doi:10.1016/j.neuron.2011.02.051 (2011).

10 Takaya, J. *et al.* A Potent and Site-Selective Agonist of TRPA1. *J Am Chem Soc* **137**, 15859-15864, doi:10.1021/jacs.5b10162 (2015).

11 Hinman, A., Chuang, H. H., Bautista, D. M. & Julius, D. TRP channel activation by reversible covalent modification. *Proc Natl Acad Sci U S A* **103**, 19564-19568, doi:10.1073/pnas.0609598103 (2006).

12 Macpherson, L. J. *et al.* Noxious compounds activate TRPA1 ion channels through covalent modification of cysteines. *Nature* **445**, 541-545, doi:10.1038/nature05544 (2007).

13 Miyake, T. *et al.* Cold sensitivity of TRPA1 is unveiled by the prolyl hydroxylation blockade-induced sensitization to ROS. *Nat Commun* **7**, 12840, doi:10.1038/ncomms12840 (2016).

14 Knowlton, W. M. & McKemy, D. D. TRPM8: from cold to cancer, peppermint to pain. *Curr Pharm Biotechnol* **12**, 68-77 (2011).

15 Caterina, M. J. *et al.* Impaired nociception and pain sensation in mice lacking the capsaicin receptor. *Science* **288**, 306-313 (2000).

16 Liedtke, W. *et al.* Vanilloid receptor-related osmotically activated channel (VR-OAC), a candidate vertebrate osmoreceptor. *Cell* **103**, 525-535 (2000).

17 Shibasaki, K., Suzuki, M., Mizuno, A. & Tominaga, M. Effects of body temperature on neural activity in the hippocampus: regulation of resting membrane potentials by transient receptor potential vanilloid 4. *J Neurosci* **27**, 1566-1575, doi:10.1523/JNEUROSCI.4284-06.2007 (2007).

18 Takayama, Y., Shibasaki, K., Suzuki, Y., Yamanaka, A. & Tominaga, M. Modulation of water efflux through functional interaction between TRPV4 and TMEM16A/anoctamin 1. *FASEB J* **28**, 2238-2248, doi:10.1096/fj.13-243436 (2014).

19 Derouiche, S., Takayama, Y., Murakami, M. & Tominaga, M. TRPV4 heats up ANO1-dependent exocrine gland fluid secretion. *FASEB J* **32**, 1841-1854, doi:10.1096/fj.201700954R (2018).

20 Viitanen, T. M., Sukumaran, P., Lof, C. & Tornquist, K. Functional coupling of TRPC2 cation channels and the calcium-activated anion channels in rat thyroid cells: implications for iodide homeostasis. *J Cell Physiol* **228**, 814-823, doi:10.1002/jcp.24230 (2013).

21 Wang, Q., Leo, M. D., Narayanan, D., Kuruvilla, K. P. & Jaggar, J. H. Local coupling of TRPC6 to ANO1/TMEM16A channels in smooth muscle cells amplifies vasoconstriction in cerebral arteries. *Am J Physiol Cell Physiol* **310**, C1001-1009, doi:10.1152/ajpcell.00092.2016 (2016).

22 Gao da, Y. *et al.* Coupling of TRPV6 and TMEM16A in epithelial principal cells of the rat epididymis. *J Gen Physiol* **148**, 161-182, doi:10.1085/jgp.201611626 (2016).

23 Miyamoto, T. *et al.* Functional role for Piezo1 in stretch-evoked Ca(2)(+) influx and ATP release in urothelial cell cultures. *J Biol Chem* **289**, 16565-16575, doi:10.1074/jbc.M113.528638 (2014).

24 Mochizuki, T. *et al.* The TRPV4 cation channel mediates stretch-evoked Ca2+ influx and ATP release in primary urothelial cell cultures. *J Biol Chem* **284**, 21257-21264, doi:10.1074/jbc.M109.020206 (2009).

25 Moore, C. *et al.* UVB radiation generates sunburn pain and affects skin by activating epidermal TRPV4 ion channels and triggering endothelin-1 signaling. *Proc Natl Acad Sci U S A* **110**, E3225-3234, doi:10.1073/pnas.1312933110 (2013).

26 Gees, M., Colsoul, B. & Nilius, B. The role of transient receptor potential cation

channels in Ca2+ signaling. *Cold Spring Harb Perspect Biol* **2**, a003962, doi:10.1101/cshperspect.a003962 (2010).

27 Aijima, R. *et al.* The thermosensitive TRPV3 channel contributes to rapid wound healing in oral epithelia. *FASEB J* **29**, 182-192, doi:10.1096/fj.14-251314 (2015).

28 Mandadi, S. *et al.* TRPV3 in keratinocytes transmits temperature information to sensory neurons via ATP. *Pflugers Arch* **458**, 1093-1102, doi:10.1007/s00424-009-0703-x (2009).

29 Yamamoto-Kasai, E. *et al.* TRPV3 as a therapeutic target for itch. *J Invest Dermatol* **132**, 2109-2112, doi:10.1038/jid.2012.97 (2012).

30 He, Y. *et al.* A gain-of-function mutation in TRPV3 causes focal palmoplantar keratoderma in a Chinese family. *J Invest Dermatol* **135**, 907-909, doi:10.1038/jid.2014.429 (2015).

31 Sokabe, T., Fukumi-Tominaga, T., Yonemura, S., Mizuno, A. & Tominaga, M. The TRPV4 channel contributes to intercellular junction formation in keratinocytes. *J Biol Chem* **285**, 18749-18758, doi:10.1074/jbc.M110.103606 (2010).

32 Park, Y. J. & Lee, H. K. The Role of Skin and Orogenital Microbiota in Protective Immunity and Chronic Immune-Mediated Inflammatory Disease. *Front Immunol* **8**, 1955, doi:10.3389/fimmu.2017.01955 (2017).

33 Barrientos, S., Stojadinovic, O., Golinko, M. S., Brem, H. & Tomic-Canic, M. Growth factors and cytokines in wound healing. *Wound Repair Regen* **16**, 585-601, doi:10.1111/j.1524-475X.2008.00410.x (2008).

34 Bill, A. & Alex Gaither, L. The Mechanistic Role of the Calcium-Activated Chloride Channel ANO1 in Tumor Growth and Signaling. *Adv Exp Med Biol* **966**, 1-14, doi:10.1007/5584_2016_201 (2017).

35 Wang, H. *et al.* Cell-specific mechanisms of TMEM16A Ca(2+)-activated chloride channel in cancer. *Mol Cancer* **16**, 152, doi:10.1186/s12943-017-0720-x (2017).

36 Cha, J. Y. *et al.* Anoctamin 1 (TMEM16A) is essential for testosterone-induced prostate hyperplasia. *Proc Natl Acad Sci U S A* **112**, 9722-9727, doi:10.1073/pnas.1423827112 (2015).

37 Deng, L. *et al.* Knockdown of TMEM16A suppressed MAPK and inhibited cell proliferation and migration in hepatocellular carcinoma. *Onco Targets Ther* **9**, 325-333, doi:10.2147/OTT.S95985 (2016).

38 Ruiz, C. *et al.* Enhanced expression of ANO1 in head and neck squamous cell carcinoma causes cell migration and correlates with poor prognosis. *PLoS One* **7**, e43265, doi:10.1371/journal.pone.0043265 (2012).

39 Suzuki, J. *et al.* Calcium-dependent phospholipid scramblase activity of TMEM16

protein family members. *J Biol Chem* **288**, 13305-13316, doi:10.1074/jbc.M113.457937 (2013).

40 Caterina, M. J. & Pang, Z. TRP Channels in Skin Biology and Pathophysiology. *Pharmaceuticals (Basel)* **9**, doi:10.3390/ph9040077 (2016).

41 Takayama, Y., Furue, H. & Tominaga, M. 4-isopropylcyclohexanol has potential analgesic effects through the inhibition of anoctamin 1, TRPV1 and TRPA1 channel activities. *Sci Rep* **7**, 43132, doi:10.1038/srep43132 (2017).

42 Takayama, Y., Uta, D., Furue, H. & Tominaga, M. Pain-enhancing mechanism through interaction between TRPV1 and anoctamin 1 in sensory neurons. *Proc Natl Acad Sci U S A* **112**, 5213-5218, doi:10.1073/pnas.1421507112 (2015).

43 Ferrera, L., Caputo, A. & Galietta, L. J. TMEM16A protein: a new identity for Ca(2+)-dependent Cl(-) channels. *Physiology (Bethesda)* **25**, 357-363, doi:10.1152/physiol.00030.2010 (2010).

44 Zhao, P. *et al.* Voltage-gated sodium channel expression in rat and human epidermal keratinocytes: evidence for a role in pain. *Pain* **139**, 90-105, doi:10.1016/j.pain.2008.03.016 (2008).

45 Reilly, J. M., Telezhkin, V., Passmore, G. M., Marsh, S. J. & Brown, D. A. Kv7/M-type potassium channels in rat skin keratinocytes. *Pflugers Arch* **465**, 1371-1381, doi:10.1007/s00424-013-1276-2 (2013).

46 Denda, M., Fujiwara, S. & Hibino, T. Expression of voltage-gated calcium channel subunit alpha1C in epidermal keratinocytes and effects of agonist and antagonists of the channel on skin barrier homeostasis. *Exp Dermatol* **15**, 455-460, doi:10.1111/j.0906-6705.2006.00430.x (2006).

47 Kinikoglu, B., Damour, O. & Hasirci, V. Tissue engineering of oral mucosa: a shared concept with skin. *J Artif Organs* **18**, 8-19, doi:10.1007/s10047-014-0798-5 (2015).

48 Rock, J. R., Futtner, C. R. & Harfe, B. D. The transmembrane protein TMEM16A is required for normal development of the murine trachea. *Dev Biol* **321**, 141-149, doi:10.1016/j.ydbio.2008.06.009 (2008).

49 Vedula, S. R., Ravasio, A., Lim, C. T. & Ladoux, B. Collective cell migration: a mechanistic perspective. *Physiology (Bethesda)* **28**, 370-379, doi:10.1152/physiol.00033.2013 (2013).

50 Cho, H. *et al.* The calcium-activated chloride channel anoctamin 1 acts as a heat sensor in nociceptive neurons. *Nat Neurosci* **15**, 1015-1021, doi:10.1038/nn.3111 (2012).

51 Xu, H. *et al.* TRPV3 is a calcium-permeable temperature-sensitive cation channel. *Nature* **418**, 181-186, doi:10.1038/nature00882 (2002).

52 Peier, A. M. *et al.* A heat-sensitive TRP channel expressed in keratinocytes. *Science* **296**, 2046-2049, doi:10.1126/science.1073140 (2002).

53 Smith, G. D. *et al.* TRPV3 is a temperature-sensitive vanilloid receptor-like protein. *Nature* **418**, 186-190, doi:10.1038/nature00894 (2002).

54 Guler, A. D. *et al.* Heat-evoked activation of the ion channel, TRPV4. *J Neurosci* **22**, 6408-6414, doi:20026679 (2002).

55 Zhong, S., Navaratnam, D. & Santos-Sacchi, J. A genetically-encoded YFP sensor with enhanced chloride sensitivity, photostability and reduced ph interference demonstrates augmented transmembrane chloride movement by gerbil prestin (SLC26a5). *PLoS One* **9**, e99095, doi:10.1371/journal.pone.0099095 (2014).

56 Blaesse, P., Airaksinen, M. S., Rivera, C. & Kaila, K. Cation-chloride cotransporters and neuronal function. *Neuron* **61**, 820-838, doi:10.1016/j.neuron.2009.03.003 (2009).

57 Ikeuchi, Y. *et al.* Measurement of [Cl(-)]i unaffected by the cell volume change using MQAE-based two-photon microscopy in airway ciliary cells of mice. *J Physiol Sci* **68**, 191-199, doi:10.1007/s12576-018-0591-y (2018).

58 Koncz, C. & Daugirdas, J. T. Use of MQAE for measurement of intracellular [Cl-] in cultured aortic smooth muscle cells. *Am J Physiol* **267**, H2114-2123, doi:10.1152/ajpheart.1994.267.6.H2114 (1994).

59 Inoue, M. *et al.* An ATP-driven Cl- pump regulates Cl- concentrations in rat hippocampal neurons. *Neurosci Lett* **134**, 75-78 (1991).

60 Gonczi, M. *et al.* Hypotonic stress influence the membrane potential and alter the proliferation of keratinocytes in vitro. *Exp Dermatol* **16**, 302-310, doi:10.1111/j.1600-0625.2006.00533.x (2007).

61 Koegel, H. & Alzheimer, C. Expression and biological significance of Ca2+-activated ion channels in human keratinocytes. *FASEB J* **15**, 145-154, doi:10.1096/fj.00-0055com (2001).

62 Mauro, T. M., Pappone, P. A. & Isseroff, R. R. Extracellular calcium affects the membrane currents of cultured human keratinocytes. *J Cell Physiol* **143**, 13-20, doi:10.1002/jcp.1041430103 (1990).

63 Pearce, A. K. & Humphrey, T. C. Integrating stress-response and cell cycle checkpoint pathways. *Trends Cell Biol* **11**, 426-433 (2001).

64 Zhang, W. & Liu, H. T. MAPK signal pathways in the regulation of cell proliferation in mammalian cells. *Cell Res* **12**, 9-18, doi:10.1038/sj.cr.7290105 (2002).

65 Sarsour, E. H., Kumar, M. G., Chaudhuri, L., Kalen, A. L. & Goswami, P. C. Redox control of the cell cycle in health and disease. *Antioxid Redox Signal* **11**, 2985-3011,

doi:10.1089/ARS.2009.2513 (2009).

66 Matsui, T. & Amagai, M. Dissecting the formation, structure and barrier function of the stratum corneum. *Int Immunol* **27**, 269-280, doi:10.1093/intimm/dxv013 (2015).

67 Woelfle, U. *et al.* Triterpenes promote keratinocyte differentiation in vitro, ex vivo and in vivo: a role for the transient receptor potential canonical (subtype) 6. *J Invest Dermatol* **130**, 113-123, doi:10.1038/jid.2009.248 (2010).

68 Lehen'kyi, V. *et al.* TRPV6 is a Ca2+ entry channel essential for Ca2+-induced differentiation of human keratinocytes. *J Biol Chem* **282**, 22582-22591, doi:10.1074/jbc.M611398200 (2007).

69 Elsholz, F., Harteneck, C., Muller, W. & Friedland, K. Calcium--a central regulator of keratinocyte differentiation in health and disease. *Eur J Dermatol* **24**, 650-661, doi:10.1684/ejd.2014.2452 (2014).

70 Bill, A. *et al.* Small molecule-facilitated degradation of ANO1 protein: a new targeting approach for anticancer therapeutics. *J Biol Chem* **289**, 11029-11041, doi:10.1074/jbc.M114.549188 (2014).

71 Rocha-Gonzalez, H. I., Mao, S. & Alvarez-Leefmans, F. J. Na+,K+,2Cl- cotransport and intracellular chloride regulation in rat primary sensory neurons: thermodynamic and kinetic aspects. *J Neurophysiol* **100**, 169-184, doi:10.1152/jn.01007.2007 (2008).

72 Kaila, K., Price, T. J., Payne, J. A., Puskarjov, M. & Voipio, J. Cation-chloride cotransporters in neuronal development, plasticity and disease. *Nat Rev Neurosci* **15**, 637-654, doi:10.1038/nrn3819 (2014).

73 Kursan, S. *et al.* The neuronal K(+)Cl(-) co-transporter 2 (Slc12a5) modulates insulin secretion. *Sci Rep* **7**, 1732, doi:10.1038/s41598-017-01814-0 (2017).

74 Patthey, C. & Gunhaga, L. Specification and regionalisation of the neural plate border. *Eur J Neurosci* **34**, 1516-1528, doi:10.1111/j.1460-9568.2011.07871.x (2011).

75 Denda, M., Inoue, K., Inomata, S. & Denda, S. gamma-Aminobutyric acid (A) receptor agonists accelerate cutaneous barrier recovery and prevent epidermal hyperplasia induced by barrier disruption. *J Invest Dermatol* **119**, 1041-1047, doi:10.1046/j.1523-1747.2002.19504.x (2002).

76 Shiozaki, A., Otsuji, E. & Marunaka, Y. Intracellular chloride regulates the G(1)/S cell cycle progression in gastric cancer cells. *World J Gastrointest Oncol* **3**, 119-122, doi:10.4251/wjgo.v3.i8.119 (2011).

77 Ohsawa, R. *et al.* Intracellular chloride regulates cell proliferation through the activation of stress-activated protein kinases in MKN28 human gastric cancer cells. *J Cell Physiol* **223**, 764-770, doi:10.1002/jcp.22088 (2010).

78 Besson, A., Dowdy, S. F. & Roberts, J. M. CDK inhibitors: cell cycle regulators and beyond. *Dev Cell* **14**, 159-169, doi:10.1016/j.devcel.2008.01.013 (2008).

79 Zhan, R. *et al.* Nitric oxide enhances keratinocyte cell migration by regulating Rho GTPase via cGMP-PKG signalling. *PLoS One* **10**, e0121551, doi:10.1371/journal.pone.0121551 (2015).

80 Rohani, M. G. & Parks, W. C. Matrix remodeling by MMPs during wound repair. *Matrix Biol* **44-46**, 113-121, doi:10.1016/j.matbio.2015.03.002 (2015).

81 Neely, E. K., Morhenn, V. B., Hintz, R. L., Wilson, D. M. & Rosenfeld, R. G. Insulin-Like Growth Factors are Mitogenic for Human Keratinocytes and a Squamous Cell Carcinoma. *Journal of Investigative Dermatology* **96**, 104-110, doi:10.1111/1523-1747.ep12515914 (1991).

82 Kroeze, K. L. *et al.* Autocrine regulation of re-epithelialization after wounding by chemokine receptors CCR1, CCR10, CXCR1, CXCR2, and CXCR3. *J Invest Dermatol* **132**, 216-225, doi:10.1038/jid.2011.245 (2012).

83 Nakajima, K., Niisato, N. & Marunaka, Y. Enhancement of tubulin polymerization by Cl(-)-induced blockade of intrinsic GTPase. *Biochem Biophys Res Commun* **425**, 225-229, doi:10.1016/j.bbrc.2012.07.072 (2012).

84 Choate, K. A., Kahle, K. T., Wilson, F. H., Nelson-Williams, C. & Lifton, R. P. WNK1, a kinase mutated in inherited hypertension with hyperkalemia, localizes to diverse Cl- -transporting epithelia. *Proc Natl Acad Sci U S A* **100**, 663-668, doi:10.1073/pnas.242728499 (2003).

85 McCormick, J. A. & Ellison, D. H. The WNKs: atypical protein kinases with pleiotropic actions. *Physiol Rev* **91**, 177-219, doi:10.1152/physrev.00017.2010 (2011).

86 Alessi, D. R. *et al.* The WNK-SPAK/OSR1 pathway: master regulator of cation-chloride cotransporters. *Sci Signal* **7**, re3, doi:10.1126/scisignal.2005365 (2014).

Figure Legends

Figure 1

TRPs and ANOs expression in NHEK

(A) RT-PCR of *TRPs* and *ANOs* in NHEK

(B) Western blot of ANO1 in NHEK. Predicted band size of ANO1 is 114 kDa.

(C and D) Calcium imaging in NHEK. Cam: Camphor, a TRPV3 agonist; GSK: GSK1016790A, a TRPV4 agonist; Cap: Capsaicin, a TRPV1 agonist; Pro: Probenecid, a TRPV2 agonist; AITC: Allyl isothiocyanate, a TRPA1 agonist; Men: Menthol, a TRPM8 agonist; OAG: 1-oleoyl acetyl-sn-glycerol, a TRPC6 agonist; Ca^{2+} (-): Calcium free bath solution.

(E) Comparison of current-voltage relationship of the currents. Red line indicates current-voltage relationship of basal current in NHEKs using the standard bath and pipette solutions. Blue line indicates current-voltage relationship in TRPV6-expressing HEK293T cells using standard bath solution and NMDG-Cl pipette solution. Holding potential was -60 mV and ramp-pulse was from -100 to +100 mV for 300 ms duration.

Figure 2

TRPV3 and ANO1 interaction in HEK293T cells

(A) Representative traces of camphor-induced currents in HEK293T cell expressing hTRPV3 and hANO1, hANO1 or hTRPV3 alone. All data were collected using an NMDG-Cl bath and pipette solution. Free calcium in pipette solution was 100 nM. Holding potential was -60 mV and ramp-pulse was from -100 to +100 mV for 300 ms duration. Dotted line indicates a current value at 0 pA.

(B) Comparison of peak currents of (A) at -60 mV (n = 5 or 6). Statistical significance was determined with a Bonferroni correction.

(C) Immunoprecipitation of ANO1 or TRPV3 and Western blot of TRPV3 in HEK293T cells transfected with *Trpv3* and *Ano1* cDNAs, *Ano1* alone, *Trpv4* alone or pcDNA3.1.

Figure 3

TRPV3 and ANO1 interaction in NHEKs

(A and B) Representative traces of camphor-induced currents in NHEKs. (A) The trace was collected using an NMDG-Cl bath solution containing 148 mM chloride. (B) The trace was collected using an NMDG-aspartate bath solution containing 4 mM

chloride. The pipette solution contained 140 mM NMDG-Cl and 100 nM free calcium. The holding potential was -60 mV and ramp-pulse was from -100 to +100 mV for 300 ms duration.

(C) Comparison of current-voltage relationships of the currents at arrowheads in (A) and (B).

(D) Calcium imaging of NHEKs upon camphor application in calcium-free conditions.

(E) Comparison of camphor-induced peak currents at -60 mV in an NMDG-Cl bath solution containing 2 mM calcium or calcium free bath solution (n = 5). Statistical significance was determined with the Student's *t*-test.

(F) Representative traces of camphor-induced currents with an ANO1 inhibitor, Ani9. The trace was collected using an NMDG-Cl bath solution containing 148 mM chloride.

Figure 4

Effect of ANO1 inhibitors on TRPV3 and TRPV4 activities

Averaged changes in intracellular calcium concentrations (indicated by ratios normalized to that caused by ionomycin) upon camphor or GSK application

(A) Calcium imaging of HEK293T cell-expressed hTRPV3 upon camphor application with or without ANO1 inhibitors, T16A or CaCC-A01.

(B) Calcium imaging of HEK293T cell-expressed hTRPV3 upon camphor application with or without ANO1 inhibitor, Ani9.

(C) Calcium imaging of HEK293T cell-expressed hTRPV4 upon GSK application with or without ANO1 inhibitors, T16A or CaCC-A01.

Figure 5

Voltage-gated calcium channel expression

(A) Representative traces of NHEKs. Step pulses for 500 msec were applied between -100 mV and +100 mV with 20 mV increments from -70 mV. Calcium base bath and pipette solutions were used.

(B) Calcium imaging of NHEKs upon 80 mM potassium bath solution (High K^+).

Figure 6

DNA microarray analysis of NHEKs

(A) Scatter Plot of signal value of each gene from NHEKs cultured in 10 μM T16-containing medium or control medium. Red dots indicate Z score > 2, blue dots indicate Z score < -2.

(B) Scatter Plot of signal value of each gene from NHEKs cultured in low chloride medium or control medium. Red dots indicate Z score > 2, blue dots indicate Z score < -2.

Figure 7

Effect of an ANO1 inhibitor in culture insert assay

(A) Schematic image of culture insert assay.

(B) Culture insert assay in medium with or without 5 μM T16A. Bright field at 0 h and calcein staining at 24 h. Washout indicates change of medium from T16A-containing medium to control medium at 12 h.

(C) Increased areas at 12 h or 24 h in the medium with or without 5 μM T16A. Data represent means ± SEM (n = 5). Statistical significance was determined with Student's *t*-test or Bonferroni correction. *, $p < 0.05$; **, $p < 0.01$.

(D) Velocity of NHEKs with or without 5 μM T16A in culture insert assay.

(E) Average velocity from (D). Each column indicates average velocity during indicated time. Data represent means ± SEM (n = 50). Statistical significance was determined with Bonferroni correction. *, $p < 0.05$; **, $p < 0.01$.

(F) MTT assay of NHEKs cultured in indicated media. Data represent means ± SEM (n = 6). Statistical significance was determined with Dunnett's test. **, $p < 0.01$.

Figure 8

Effect of temperature on the in the culture insert assay

Measurements of increased areas at 24 h at indicated temperatures. Data represent means ± SEM (n = 10). Statistical significance was determined with an independent *t*-test or Bonferroni correction. *, $p < 0.05$ by Bonferroni correction; **, $p < 0.01$ Bonferroni correction; ## $p < 0.01$, *t*-test (vs corresponding Cont).

Figure 9

Effect of a low chloride medium in the in the culture insert assay

(A) Culture insert assay in the low chloride medium or control medium. Bright fields at 0 h and calcein staining at 24 h. Control 12h indicates a change of medium from low chloride medium to control medium at 12 h.

(B) Measurements of increased areas at 12 h or 24 h in the low chloride medium or control medium. Data represent means ± SEM (n = 6). Statistical significance was determined with Student's *t*-test or Bonferroni correction.

*, $p < 0.05$; **, $p < 0.01$.

Figure 10

Expression of cation-chloride cotransporters and calculated chloride concentrations in NHEKs

(A) RT-PCR assessment of cation-chloride cotransporter genes in NHEKs.

(B) Representative picture of chloride ion-quenched fluorescent indicator, MQAE in NHEKs.

(C) Calibration curve and calculated intracellular chloride concentration in NHEKs. Calibration curve was made by Stern-Volmer plot, $F_0/F = 1 + K_q[Cl]$. F_0: fluorescence intensity at 0 mM chloride, F: fluorescence intensity at each chloride concentration, K_q: extinction coefficient.

Figure 11

Effect of an ANO1 inhibitor and a low chloride medium on MAP kinase phosphorylation

(A) Schematic representation of MAP kinase signaling.

(B) Western blotting of total MAP kinase and phosphorylated MAP kinase.

Figure 12

Effect of an ANO1 inhibitor on NHEK differentiation

RT-PCR of differentiation marker genes in NHEKs

KRT1: keratin 1, *IVL*: involucrin, *TGM1*: transglutaminase 1

Differentiation was induced by the following conditions.

Mild: cultured at medium cell density in 0.15 mM calcium medium for 2 days.

Differentiated: cultured at high cell density in 1.5 mM calcium medium for 3 days.

Undifferentiated: cultured at low cell density in 0.15 mM calcium medium for 3 days.

Treatment with 10 μM T16 was done for 13 h.

Figure 13

Cell cycle analysis of NHEK

(A) Representative picture of redox dye staining for cell cycle analysis.

(B) Representative pictures of each phase cell (red) in the presence or absence of 5 μM T16A.

(C) Comparison of rate of each phase cell. Data represent means ± SEM (n = 7). Statistical significance was determined with Bonferroni correction. *, $p < 0.05$; **, $p < 0.01$.

Tables

Table 1

Primer list for reverse transcription-PCR (RT-PCR)

All primers span an exon-exon junction.

	Forward primer	Reverse primer
TRPV1	CTGCGGACCCACTCCAAAAGGA	AGAGCAGCAGGCTCTCCAGATC
TRPV2	CTGCACATCGCCATTGAGAAGA	TTGGAGGAGCCCATCATACATG
TRPV3	GCTGAAGAAGCGCATCTTTGCA	TCATAGGCCTCCTCTGTGTACT
TRPV4	TACCTGTGTGCCATGGTCATCT	TGCTATAGGTCCCCGTCAGCTT
TRPV5	GTCCCAGCCCCAAATAGACC	GCAGTCTGACCTGCAAAAGC
TRPV6	GTAGAAGTGGCCTAGCTCCTCGG	AGCCTACATGACCCCTAAGGACG
TRPA1	GACCACAATGGCTGGACAGCT	GTACCATTGCGTTGAGGGCTGT
TRPM8	CCTGTTCCTCTTTGCGGTGTGGAT	TCCTCTGAGGTGTCGTTGGCTTT
β-actin	GATCCTCACCGAGCGCGGCTACA	GCGGATGTCCACGTCACACTTCA
ANO1	GAGATCGGTTCCCAGCCTAC	GGGACCTCGATCTTGGTGAG
ANO2	TTCATGGCTCTGTGGGCTAC	GCAGACTGGTTGCTCTCCTT
ANO3	CGTAGGCCACCCAGGAAAAT	CCAGTTCTGGATCAACGGGT
ANO4	GAGAAGCTGGGCAAAAGTGC	GTGCTTTTGCACAGCCAGAA
ANO5	GAGTGAGAGCCTGAGCAGC	TTCCGCCTTTAACTCTGCGT
ANO6	CGAACCCCGGAGTTTGAAGA	CTCCCATGGTGCGTGTACTT
*ANO7*s	CAAGCCCCGGATCGACTTC	CATGACAGCCTCCACGTACC
*ANO7*l	AGGAGCCGGGAAGCCTTG	TGGTTGGGTAACTCCTGCAA
ANO8	CGGGCCGTCCGTAGC	TCATCGGTCGTGTCTGGGAAG
ANO9	TCTTTGGGATCCGTGCTGAC	GGGTGAGCTTGGCAAAAGTG
ANO10	TCTTTCACACCTTTGGTGGTCA	TGCCAGACGTGAGCAATCTT
NKCC2	GGCTCCATCACAGTGGTGAT	TGGGGATCCTCCAAATCTCCT
NKCC1	TTTGCAGAAACCGTGGTGGA	GCTGACTGAGGATCTGCAAG
NCC	TTTGACGATGGAGGCCTCAC	CTGCCGAAGGGACTTGACTC
KCC1	CGGCAGATGAGACTGACCAA	CCAGGCCACAAGATGACACT
KCC2	AAGCCGGACCAATCCAATGT	CTGTTACCCCAGACCACAGC
KCC3	GCACTCTTTGAGGAAGAAATGGAC	GCTGGCACCACTCCATTAGT
KCC4	CGTTTCCGCAAAACCAGGAG	TTCCTGTCGTGGATCAGCTG

Table 2

Comparison of expression of wound healing-related or chloride-sensing gene
Low Cl^-/Cont: the ratio of gene expression in low chloride condition to control condition
T16A/Cont: the ratio of gene expression in T16A-treated condition to control condition
Blue color indicates Z score < -2.

Description	GeneSymbol	Low Cl^- /Cont	T16A /Cont
Homo sapiens matrix metallopeptidase 7	*MMP7*	0.07	0.10
Homo sapiens chemokine ligand 10	*CXCL10*	0.19	0.04
Homo sapiens insulin-like growth factor 2	*IGF2*	0.03	0.04
Homo sapiens nitric oxide synthase 2, inducible	*NOS2*	0.23	0.08
Homo sapiens WNK lysine deficient protein kinase 2	*WNK2*	0.01	0.01
Homo sapiens WNK lysine deficient protein kinase 1	*WNK1*	0.86	0.88

Figure 1

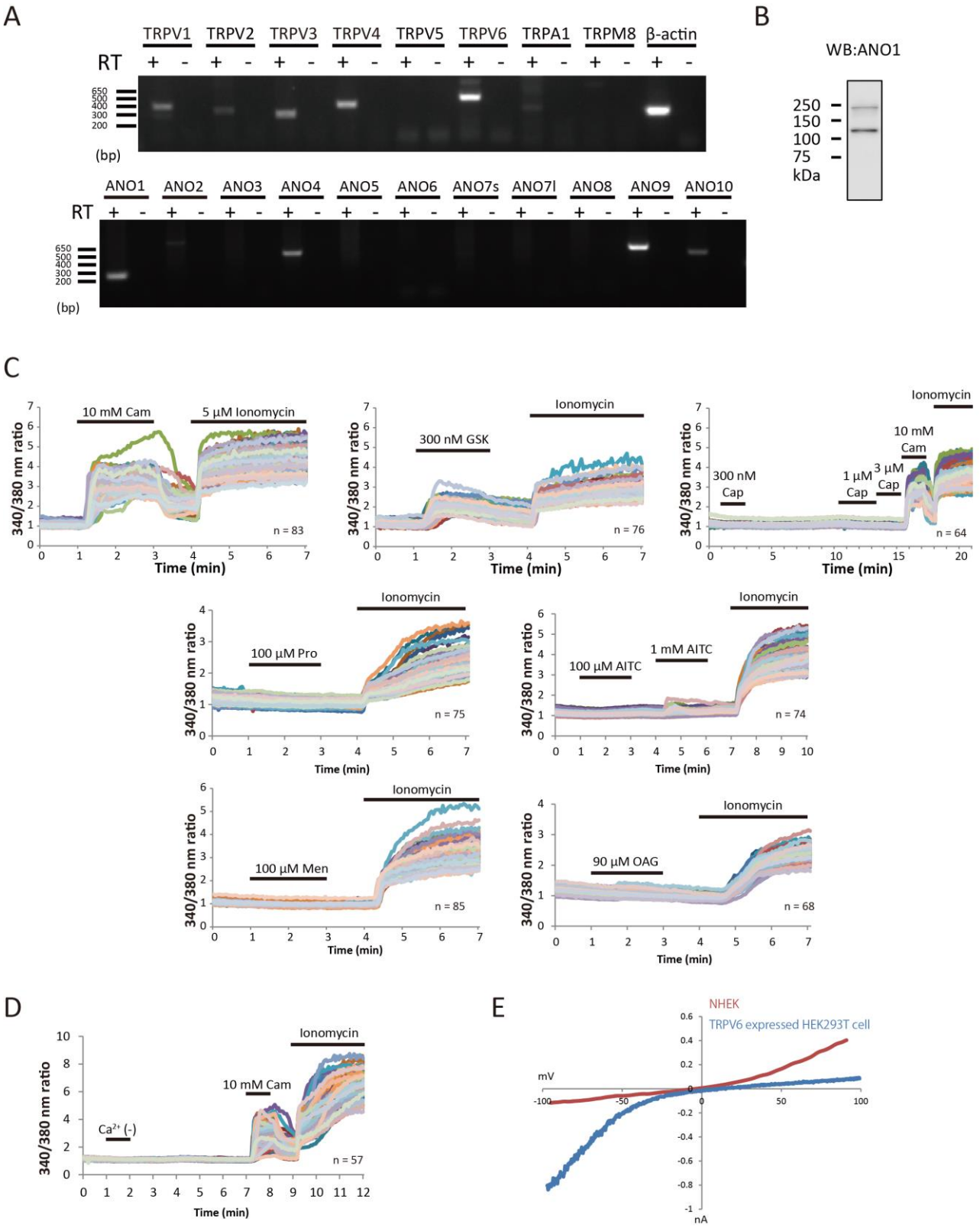
A
TRPV1 TRPV2 TRPV3 TRPV4 TRPV5 TRPV6 TRPA1 TRPM8 β-actin
RT + - + - + - + - + - + - + - + - + -
650 500 400 300 200
(bp)
ANO1 ANO2 ANO3 ANO4 ANO5 ANO6 ANO7s ANO7l ANO8 ANO9 ANO10
RT + - + - + - + - + - + - + - + - + - + -
650 500 400 300 200
(bp)
B
WB:ANO1
250 150 100 75 kDa
C
10 mM Cam
5 μM Ionomycin
n = 83
300 nM GSK
Ionomycin
n = 76
300 nM Cap
1 μM Cap
3 μM Cap
10 mM Cam
Ionomycin
n = 64
100 μM Pro
Ionomycin
n = 75
100 μM AITC
1 mM AITC
Ionomycin
n = 74
100 μM Men
Ionomycin
n = 85
90 μM OAG
Ionomycin
n = 68
340/380 nm ratio
Time (min)
D
Ca2+ (-)
10 mM Cam
Ionomycin
n = 57
340/380 nm ratio
Time (min)
E
NHEK
TRPV6 expressed HEK293T cell
mV
nA

Figure 2

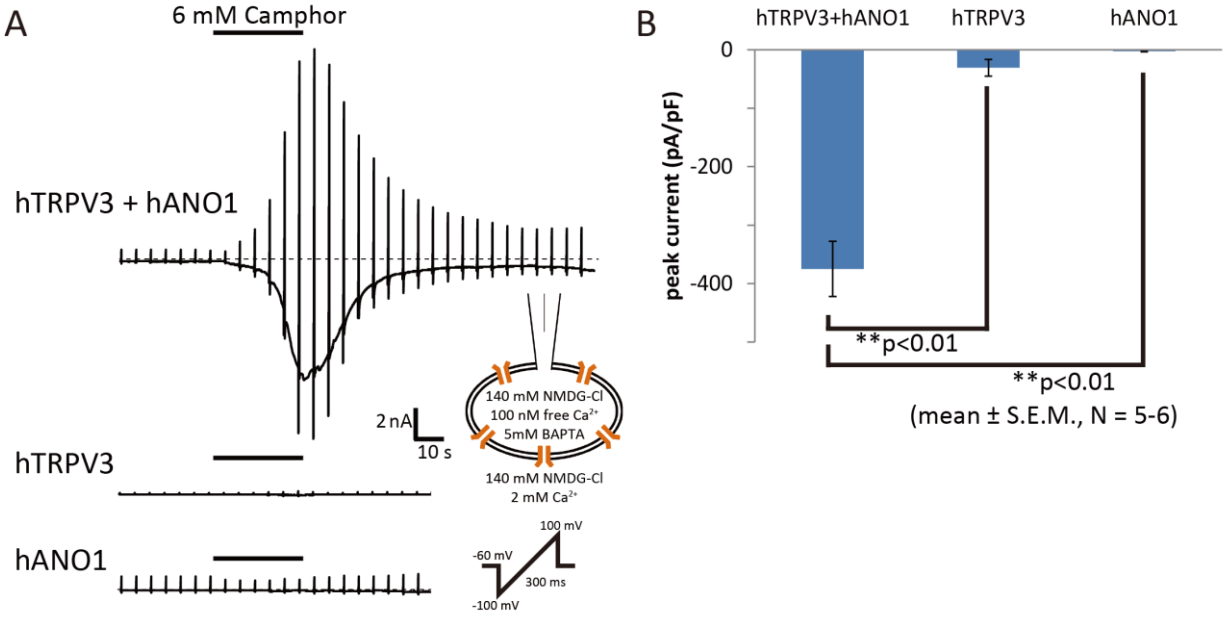
A
6 mM Camphor
hTRPV3 + hANO1
hTRPV3
hANO1
2 nA
10 s
140 mM NMDG-Cl
100 nM free Ca2+
5mM BAPTA
140 mM NMDG-Cl
2 mM Ca2+
100 mV
-60 mV
300 ms
-100 mV
B
hTRPV3+hANO1
hTRPV3
hANO1
0
-200
-400
peak current (pA/pF)
**p<0.01
**p<0.01
(mean ± S.E.M., N = 5-6)

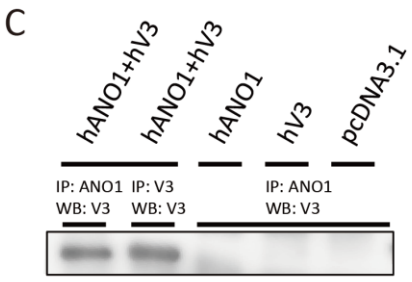
C
hANO1+hV3
hANO1+hV3
hANO1
hV3
pcDNA3.1
IP: ANO1
WB: V3
IP: V3
WB: V3
IP: ANO1
WB: V3

Figure 3

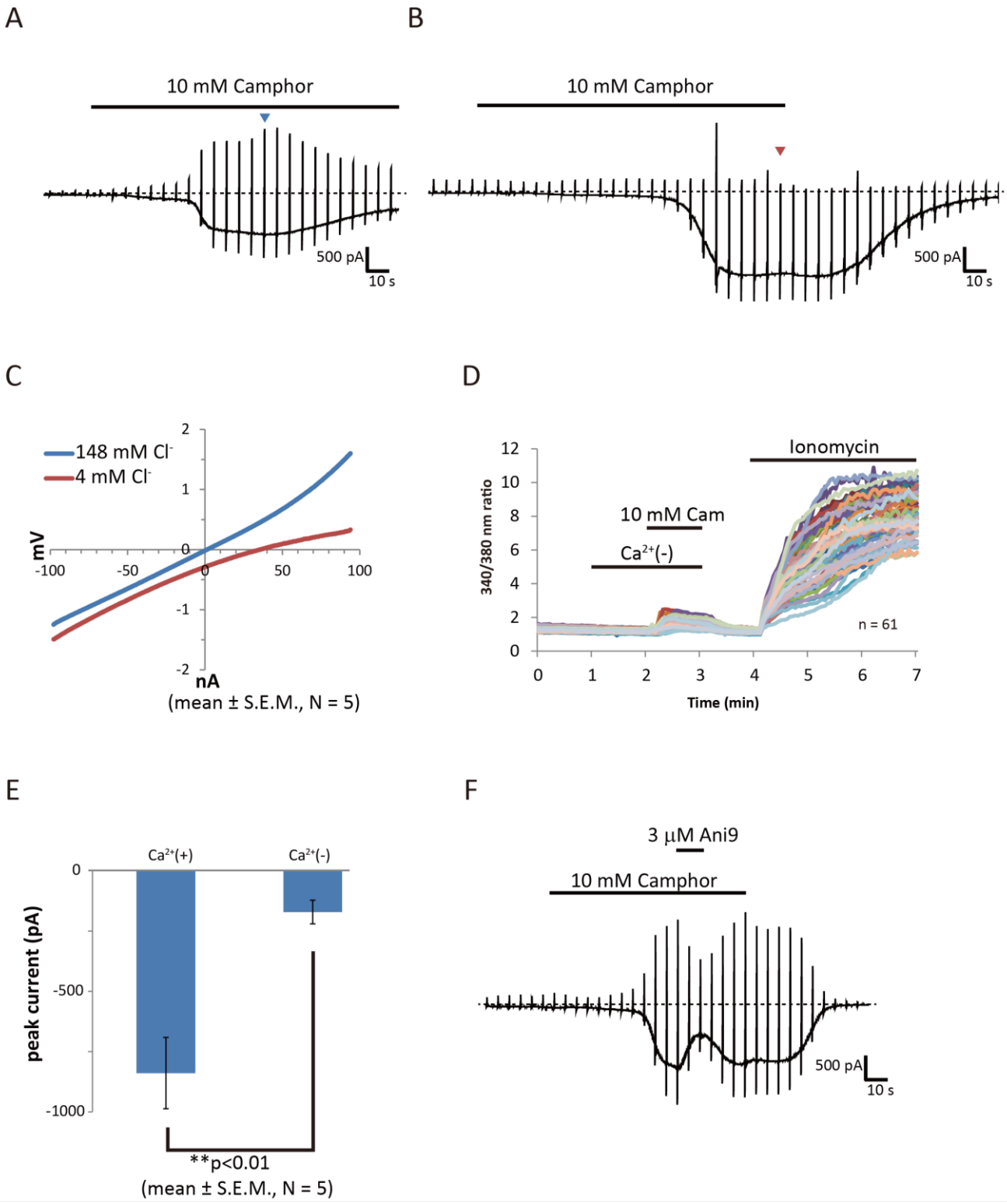
A
10 mM Camphor
500 pA
10 s
B
10 mM Camphor
500 pA
10 s
C
148 mM Cl-
4 mM Cl-
mV
nA
(mean ± S.E.M., N = 5)
D
Ionomycin
10 mM Cam
Ca2+(-)
340/380 nm ratio
n = 61
Time (min)
E
Ca2+(+)
Ca2+(-)
peak current (pA)
**p<0.01
(mean ± S.E.M., N = 5)
F
3 µM Ani9
10 mM Camphor
500 pA
10 s

Figure 4

A

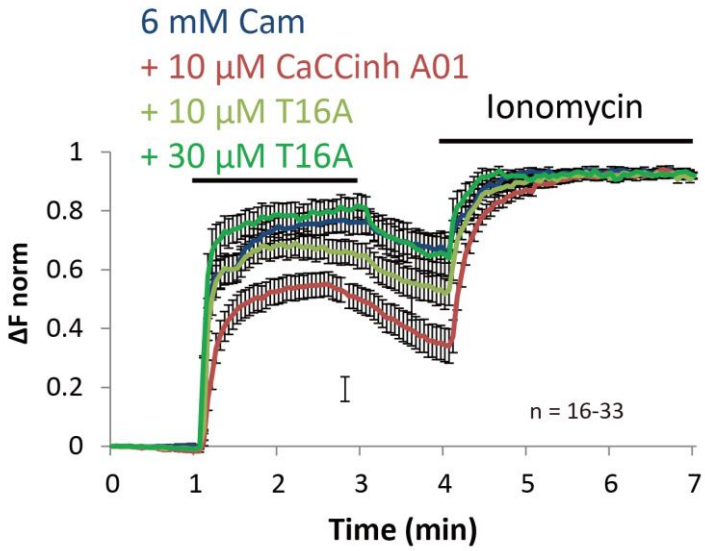
6 mM Cam
+ 10 µM CaCCinh A01
+ 10 µM T16A
+ 30 µM T16A
Ionomycin
ΔF norm
Time (min)
n = 16-33

B

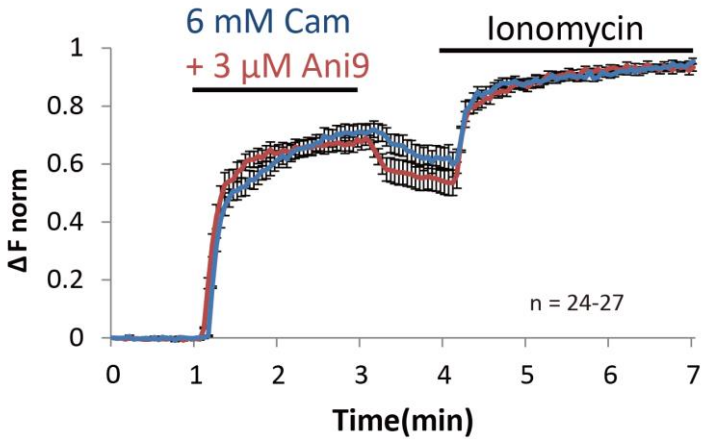
6 mM Cam
+ 3 µM Ani9
Ionomycin
ΔF norm
Time(min)
n = 24-27

C

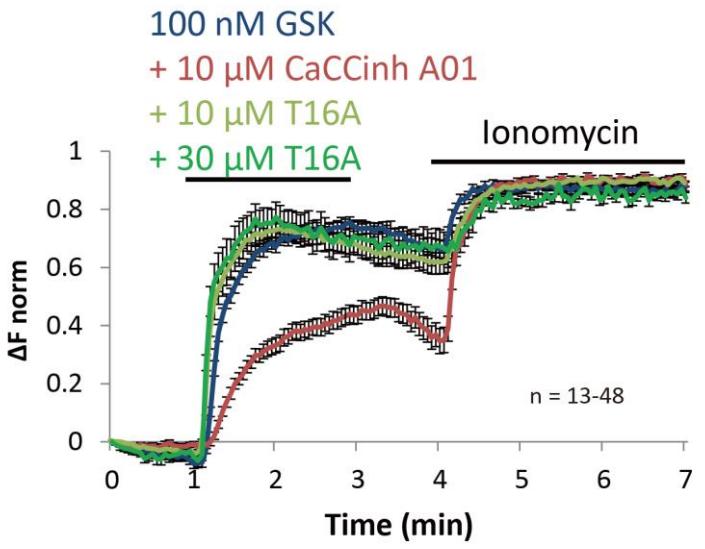
100 nM GSK
+ 10 µM CaCCinh A01
+ 10 µM T16A
+ 30 µM T16A
Ionomycin
ΔF norm
Time (min)
n = 13-48

Figure 5

A

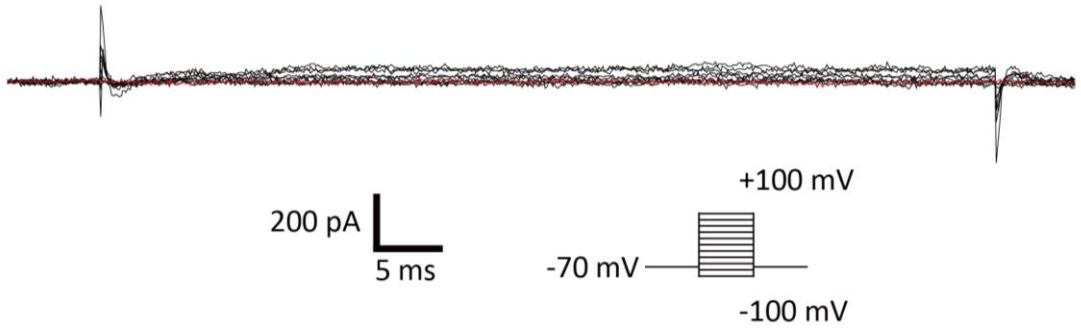
200 pA
5 ms
+100 mV
-70 mV
-100 mV

B

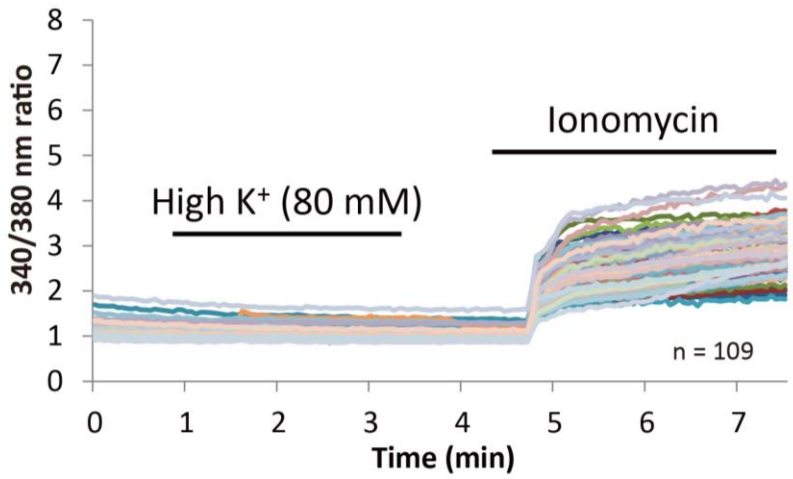
340/380 nm ratio
Ionomycin
High K⁺ (80 mM)
n = 109
Time (min)

Figure 6

A

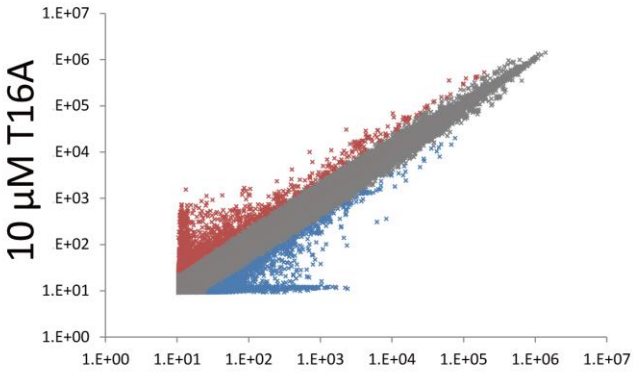

Cont

$Red_{(Z\text{-score} > 2)}$: 1766 (2.7%)
Grey: 57716
$Blue_{(Z\text{-score} < -2)}$: 1419 (2.3%)

B

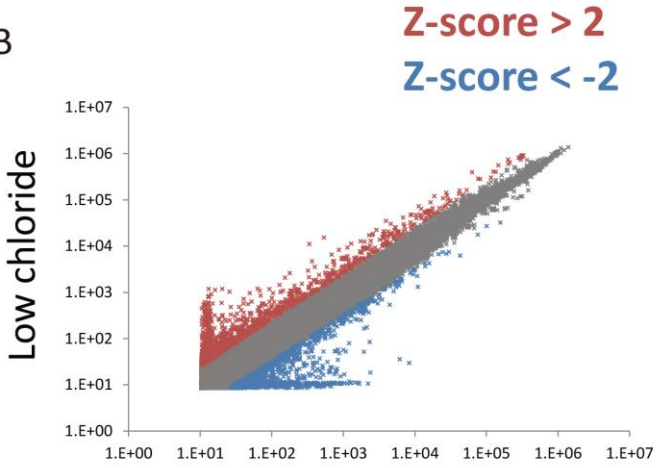

Cont

$Red_{(Z\text{-score} > 2)}$: 1617 (2.9%)
Grey: 57874
$Blue_{(Z\text{-score} < -2)}$: 1410 (2.3%)

C

T16A (ANO1 inhibitor)

Low chloride

	Red	Blue
Red	297	25
Blue	17	643

Figure 7

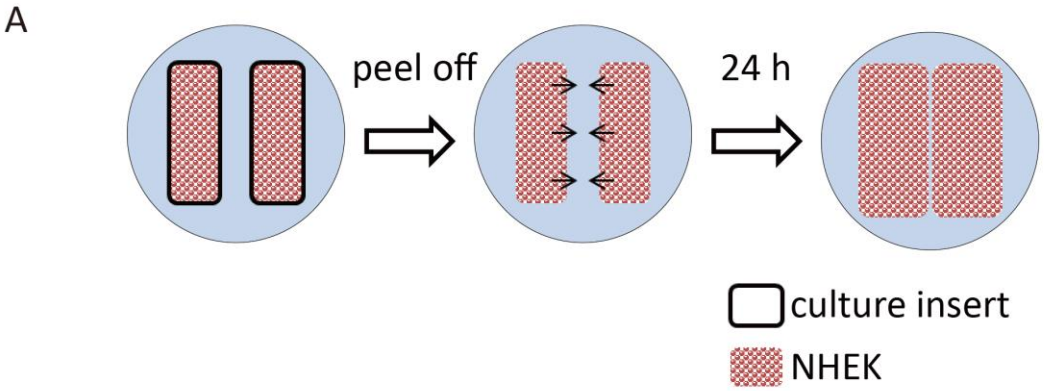
A
peel off
24 h
culture insert
NHEK

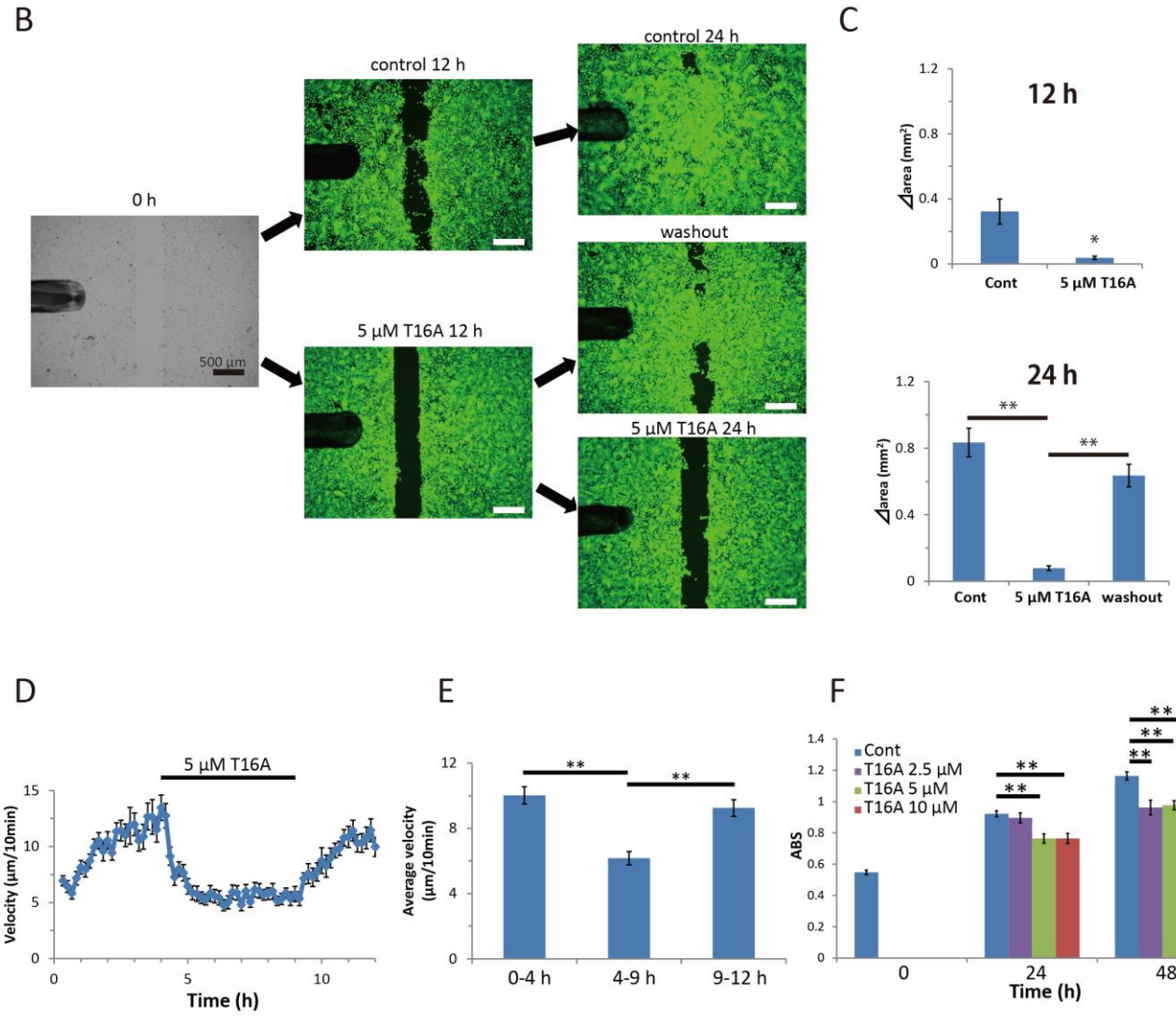
B
0 h
500 µm
control 12 h
control 24 h
5 µM T16A 12 h
washout
5 µM T16A 24 h
C
12 h
Δarea (mm²)
Cont
5 µM T16A
24 h
Cont
5 µM T16A
washout

D
5 µM T16A
Velocity (µm/10min)
Time (h)
E
Average velocity (µm/10min)
0-4 h
4-9 h
9-12 h
F
Cont
T16A 2.5 µM
T16A 5 µM
T16A 10 µM
ABS
Time (h)

Figure 8

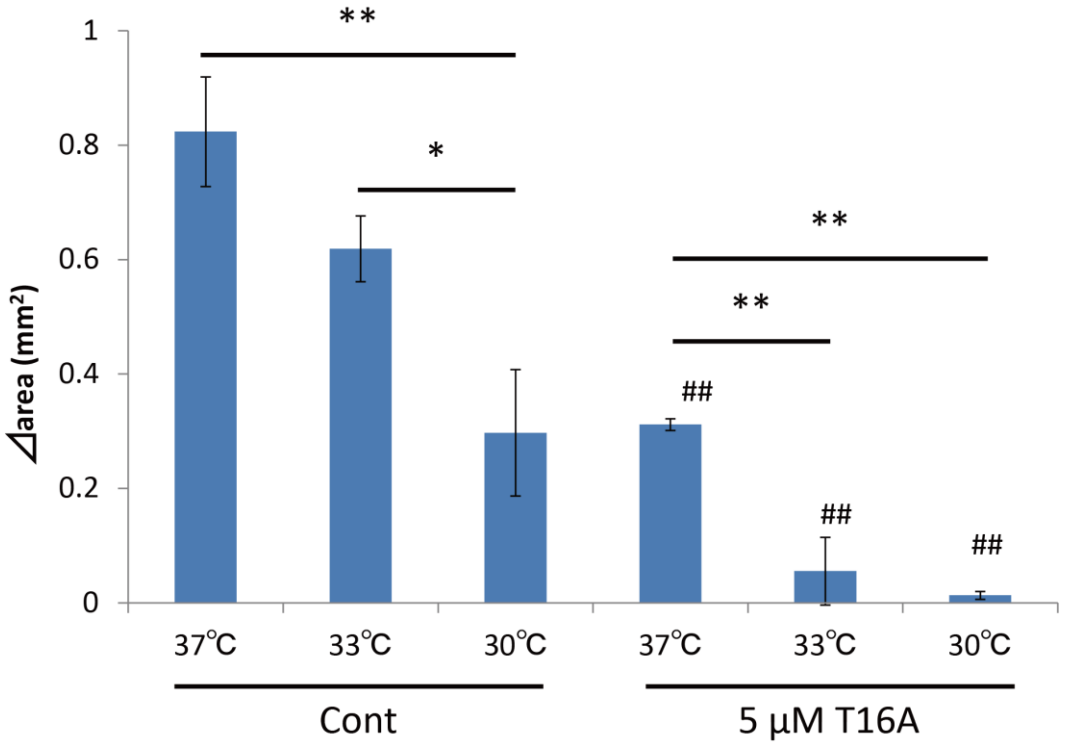

Figure 9

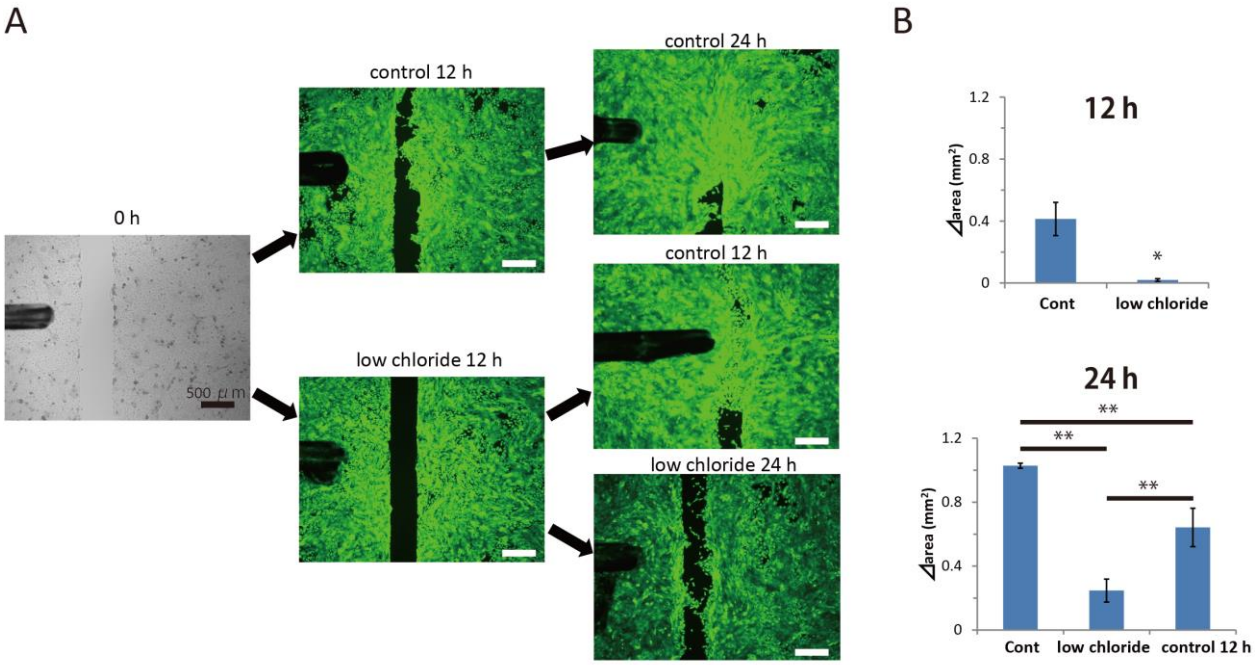
A
0 h
500 μm
control 12 h
control 24 h
low chloride 12 h
control 12 h
low chloride 24 h
B
12 h
Δarea (mm²)
1.2
0.8
0.4
0
*
Cont
low chloride
24 h
**
**
**
Cont
low chloride
control 12 h

Figure 10

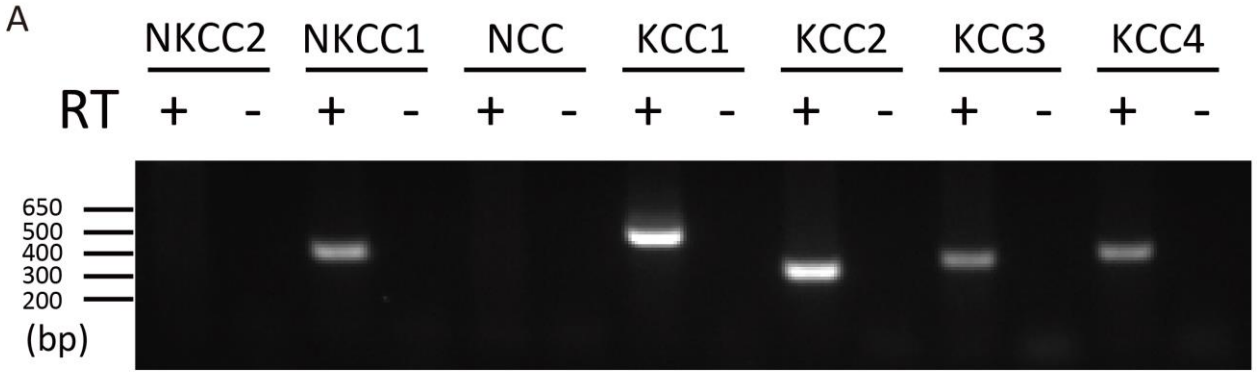
A
NKCC2
NKCC1
NCC
KCC1
KCC2
KCC3
KCC4
RT + - + - + - + - + - + - + -
650
500
400
300
200
(bp)

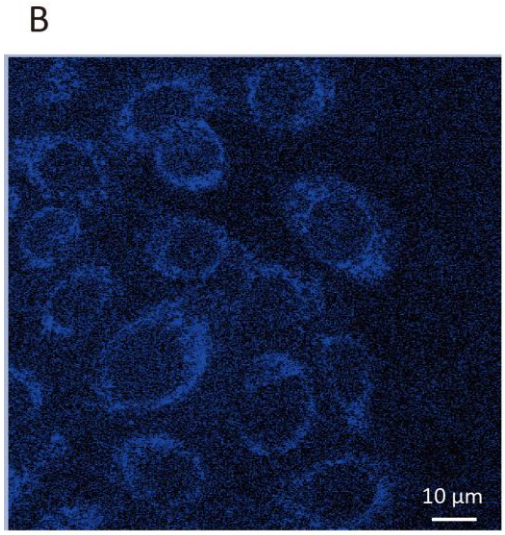
B
10 µm

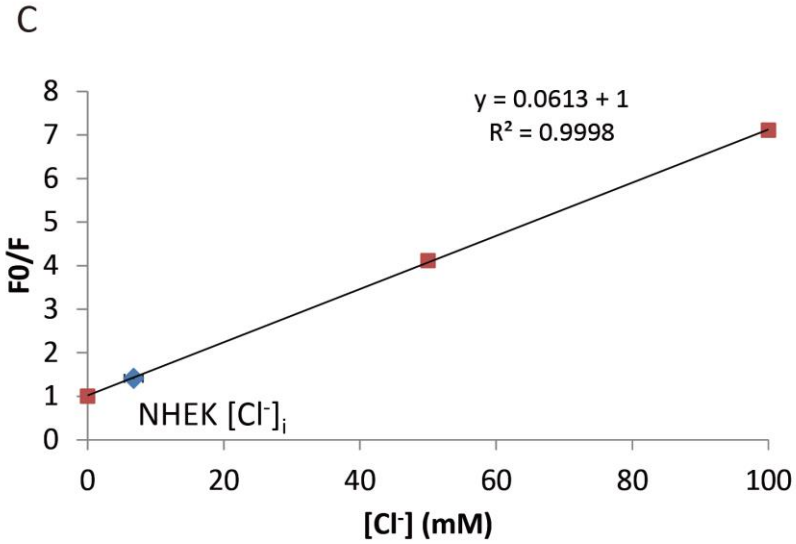
C
y = 0.0613 + 1
R² = 0.9998
F0/F
[Cl-] (mM)
NHEK [Cl-]i
0
1
2
3
4
5
6
7
8
0
20
40
60
80
100

Figure 11

A

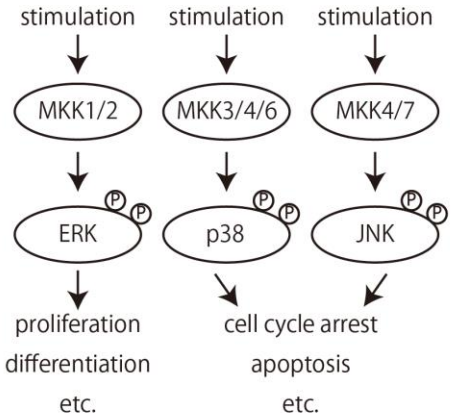
stimulation
stimulation
stimulation
MKK1/2
MKK3/4/6
MKK4/7
ERK
p38
JNK
P
P
proliferation
differentiation
etc.
cell cycle arrest
apoptosis
etc.

B

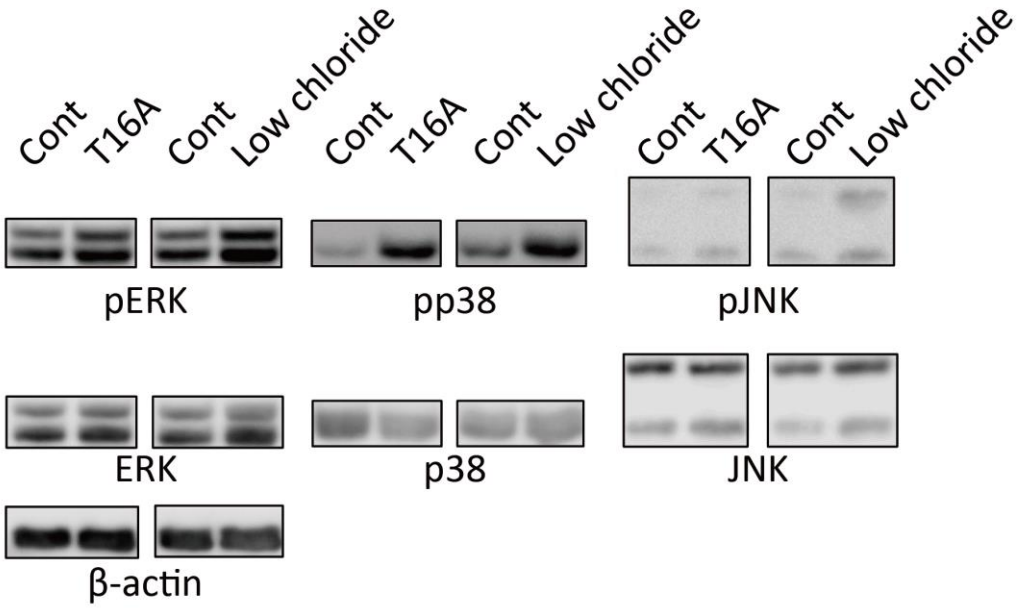
Cont
T16A
Cont
Low chloride
Cont
T16A
Cont
Low chloride
Cont
T16A
Cont
Low chloride
pERK
pp38
pJNK
ERK
p38
JNK
β-actin

Figure 12

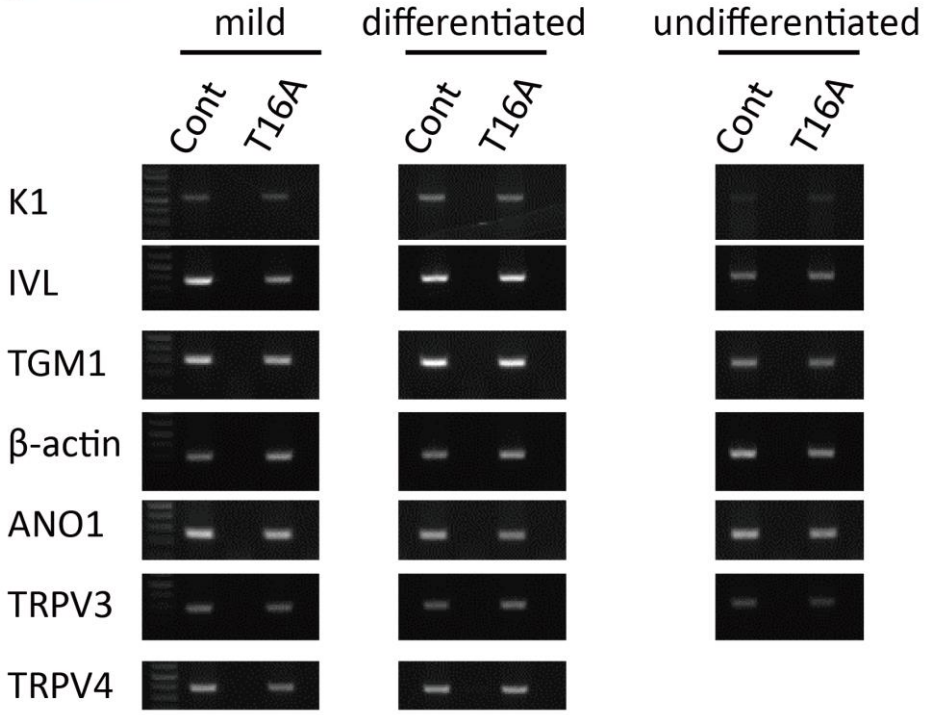
mild
differentiated
undifferentiated
Cont
T16A
Cont
T16A
Cont
T16A
K1
IVL
TGM1
β-actin
ANO1
TRPV3
TRPV4

Figure 13

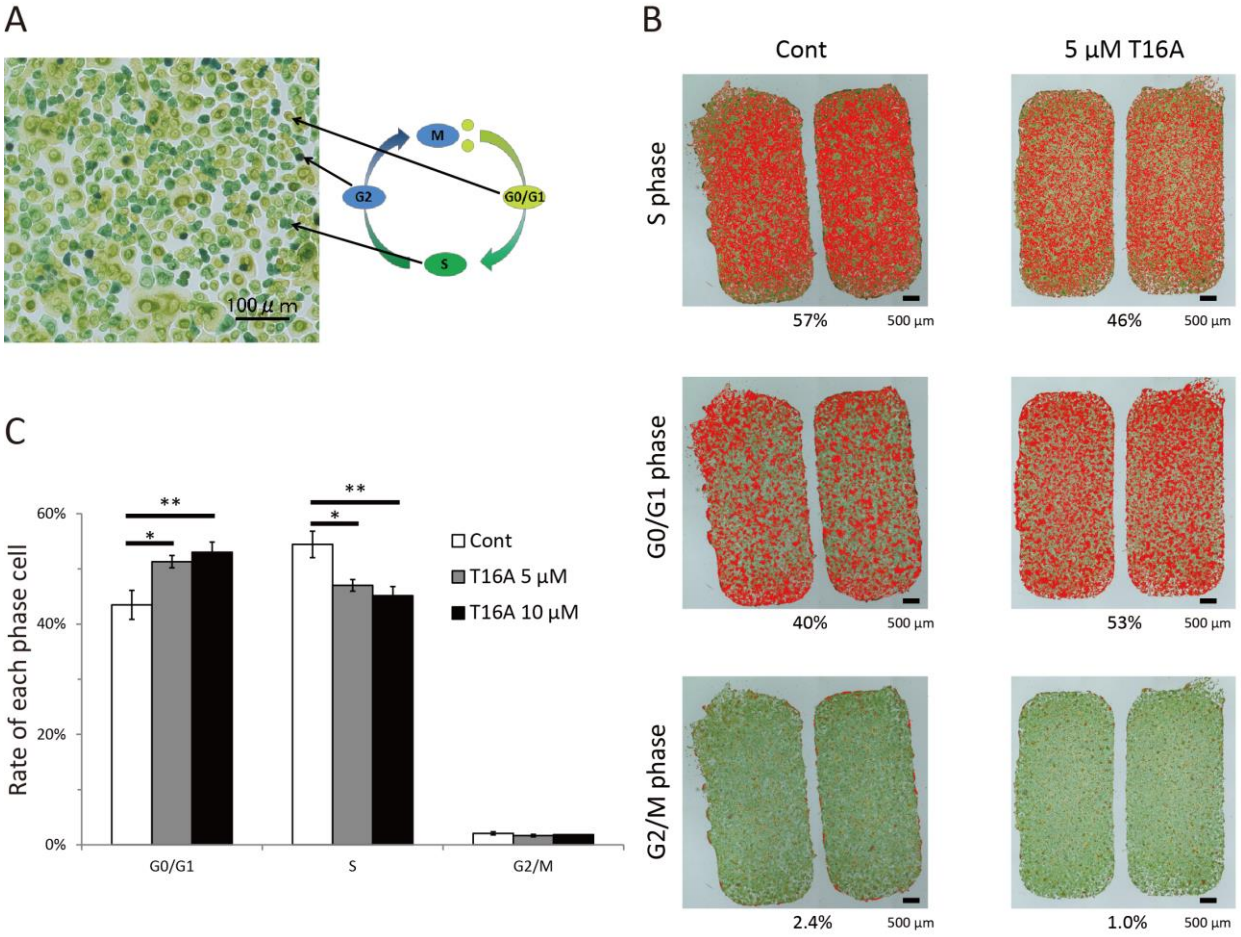
A
M
G2
G0/G1
S
100 μ m
B
Cont
5 μM T16A
S phase
57%
500 μm
46%
500 μm
G0/G1 phase
40%
500 μm
53%
500 μm
G2/M phase
2.4%
500 μm
1.0%
500 μm
C
Rate of each phase cell
60%
40%
20%
0%
**
*
**
*
Cont
T16A 5 μM
T16A 10 μM
G0/G1
S
G2/M